Title:

DNA-PK interacts with cyclic dinucleotides and inhibits type I Interferon responses

Running Title:

DNA-PK traps cyclic dinucleotides

Authors :

Isabelle K. Vila[1#], Yasmine Messaoud-Nacer[1#], Clara Taffoni[1#], Jane Jardine[2], Roger J. Eloiflin[1], Adeline Augereau[1], Soumyabrata Guha[1], Moritz Schussler[1], Pierre Le Hars[1] ,Joe McKellar[1], Tamara Carvalho[3], Jeanne Postal[4,5], Morgane Chemarin[1], Joanna Re[1], Florence Guivel-Benhassine[4,5], Raphaëlle Lopez[3], Kilian Trillet[2], Jennifer Barrat[1], Maximin Serbier[1], Insaf El Mansouri[1], Charlotte Luchsinger[6], George P. Chrousos[7], Françoise Porrot[4,5], Felipe Diaz-Griffero[6], Olivier Schwartz[4], Fabien P. Blanchet[3], Karim Majzoub[1], Nicolas Bidère[2], Dimitrios Vlachakis[7,8,9,*], Nadine Laguette[1,*]

Affiliations :

[1] Institut de Génétique Moléculaire de Montpellier (IGMM), université de Montpellier, CNRS UMR5535, Montpellier, France

[2] Team SOAP, CRCI2NA, Nantes Université, Inserm, CNRS, Université d'Angers Nantes France, Equipe Labellisée Ligue Contre le Cancer, Paris, France

[3] Institut de Recherche en Infectiologie de Montpellier (IRIM), Université de Montpellier, CNRS UMR9004, Montpellier, France

[4] Institut Pasteur, Virus and Immunity Unit, Université Paris Cité, Paris, France

[5] Vaccine Research Institute, Créteil, France.

[6] Department of Microbiology and Immunology, Albert Einstein College of Medicine, Bronx, NY 10461, USA

[7] University Research Institute of Maternal and Child Health & Precision Medicine, and UNESCO Chair on Adolescent Health Care, National and Kapodistrian University of Athens, “Aghia Sophia” Children's Hospital, 11527 Athens, Greece

[8] Laboratory of Genetics, Department of Biotechnology, School of Applied Biology and Biotechnology, Agricultural University of Athens, 75 Iera Odos, 11855 Athens, Greece

[9] School of Informatics, Faculty of Natural & Mathematical Sciences, King's College London, WC2R 2LS, Bush House, Strand, London, U.K.

[#]Equal contribution

*Correspondence to: Nadine Laguette : nadine.laguette@igmm.cnrs.fr; and Dimitrios Vlachakis : dimitris@aua.gr

Abbreviations :

2’3’-cGAMP: 2’3’-cyclic guanosine monophosphate-adenosine monophosphate or cyclic [G(2’,5’)pA(3’,5’)p]; 3’3’-cGAMP: 3’3’-cyclic guanosine monophosphate-adenosine monophosphate or cyclic [G(3',5')pA(3',5')p; CCL5: Chemokine (C-C motif) ligand 5; c-di-AMP: bis-(3'-5')-cyclic dimeric adenosine monophosphate; c-di-GMP: bis-(3'-5')-cyclic dimeric guanosine monophosphate; CDN: Cyclic dinucleotides; cGAS: cyclic GMP-AMP synthase; CXCL10: C-X-C motif chemokine ligand 10; DNA-PK= DNA-dependent protein kinase; DNA-PKcs: DNA-dependent protein kinase catalytic subunit; IFIT1/2: Interferon Induced Protein With Tetratricopeptide Repeats 1/2; IFNAR: Interferon-α/β receptor; IFNB1: Interferon beta; IFN: Interferon; IRF3: Interferon Regulatory Factor 3; ISG15: Interferon-stimulated gene 15; STING: Stimulator of Interferon Genes; TBK1= Tank Binding Kinase 1

Summary

Inflammatory signal termination is critical for the maintenance of homeostasis. Cyclic dinucleotides (CDN) are second messengers that trigger inflammatory responses through the activation of the Stimulator of Interferon Genes (STING) signaling platform. No broad-acting direct regulator of intracellular CDNs has been identified in mammals to date. We show that the DNA-dependent protein kinase catalytic subunit (DNA-PKcs), a major DNA damage response actor, directly interacts with the intracellular 2'3'-cGAMP CDN through its kinase domain, tempering STING activation. DNA-PKcs also acts on the 3'3'-cGAMP bacterial CDN and pharmacological STING agonists, impacting their bioactivity and ability to mount optimal antiviral responses. STING agonism has been considered as a therapeutic avenue to alleviate immunosuppression in human pathologies. By uncovering DNA-PKcs as a CDN signaling modulator and CDNs as inhibitors of DNA-PKcs kinase activity, we provide critical insights into CDN regulation, with implications for the development of STING-targeting therapeutics.

Main text

The presence of dsDNA in the cytosol is sensed as a danger signal and promotes the activation of inflammatory responses (Decout et al., 2021). A major pathway involved in the detection of cytosolic dsDNA relies on the cyclic GMP-AMP (cGAMP) synthase (cGAS) (Sun et al., 2013) that catalyzes the production of the 2'3'-cGAMP cyclic dinucleotide (CDN), which in turn binds and activates the Stimulator of Interferon Genes (STING) adaptor protein (Sun et al., 2013). The interaction of 2'3'-cGAMP with STING drives the assembly of a signalosome where the Tank Binding Kinase 1 (TBK1) catalyzes phosphorylation-dependent activation of transcription factors, such as the Interferon Regulatory Factor 3 (IRF3), to drive the expression of inflammatory cytokines and type I Interferons (IFNs) (Sun et al., 2009, Zhong et al., 2008). Activation of the cGAS-STING signaling axis is essential in response to pathogen infection, cellular stress, or tissue damage, which are contexts where immune stimulatory dsDNAs are exposed in the cytosol. However, chronic activation of this signaling pathway is reported in several human pathologies, such as auto-inflammatory diseases or cancer, where it is responsible for chronic low-grade disease-promoting inflammation, leading to immune dysfunction and tissue damage (Decout et al., 2021).

To mitigate the deleterious effects of unwanted activation of the cGAS-STING pathway, several regulatory layers have been described to directly control cGAS and/or STING activation (Hertzog and Rehwinkel, 2020, Vila et al., 2022). In contrast, few mammalian direct regulators of the 2'3'-cGAMP molecule have been documented (Hou et al., 2023, Li et al., 2014, Mardjuki et al., 2024), all of which acting on extracellular 2'3'-cGAMP. This is striking

since 2’3’-cGAMP is an essential component of the cGAS-STING axis which is notably involved in signal amplification and propagation (Jutte et al., 2021) and its intracellular negative regulation could be essential for signal termination. Additionally, despite several CDNs of bacterial origin being active in mammalian cells (McWhirter et al., 2009, Woodward et al., 2010), no cellular mechanism ensuring their regulation has been described to date.

Prior to the identification of cGAS, the DNA-PK holoenzyme was proposed to operate as a cytosolic dsDNA sensor (Ferguson et al., 2012). DNA-PK is comprised of three subunits, with the KU70 and KU80 scaffold proteins forming heterodimers, that ensure the recruitment of the DNA-PK catalytic subunit (DNA-PKcs) to nuclear double-strand breaks and their repair by non-homologous end-joining (Yue et al., 2020). Several studies support a role of DNA-PKcs in innate immune activation in the presence of cytosolic dsDNA, both through direct detection of cytosolic dsDNAs (Burleigh et al., 2020, Morales et al., 2017, Scutts et al., 2018, Taffoni et al., 2023) or as a co-activation of cGAS (Hristova et al., 2024, Taffoni et al., 2023) following viral infections or genotoxic stress. Yet, absence of DNA-PKcs was also shown to lead to a potentiation of type I IFN responses (Sun et al., 2020), suggesting dichotomous functions of DNA-PKcs in the regulation of cGAS-STING-associated inflammatory responses and highlighting a lack of mechanistic insight into the relationship between those two pathways.

Here, we show that DNA-PKcs acts as a direct regulator of intracellular levels of the 2’3’-cGAMP CDN. We also uncover that the action of DNA-PKcs on 2’3’-cGAMP takes place downstream of its role in the primary detection of cytosolic dsDNA, and serves as a signal terminator downstream of 2’3’-cGAMP production. We demonstrate that DNA-PKcs is also capable of regulating the bioactivity of the bacterial 3’3’-cGAMP CDN and of specific synthetic STING agonists. This finding therefore bears important implications, for our understanding of the regulation of the cGAS-STING pathway regulation, but also for the development and use of STING agonists in immunosuppressed contexts.

DNA-PKcs interacts with 2’3’-cGAMP

Since absence of DNA-PKcs was shown to promote type I IFN responses, suggesting an inhibitory function downstream of cGAS activation (Sun et al., 2020), we hypothesized that it may directly modulate 2’3’-cGAMP bioactivity. We thus tested whether DNA-PKcs interacts with 2’3’-cGAMP.

We performed *in vitro* binding assays, using a FLAG-tagged WT-DNA-PKcs (FLAG-DNA-PKcs; Figure 1A) which was FLAG-purified in conditions where the KU scaffold proteins are not detectable (Figure 1B). We found a significant enrichment of 2’3’-cGAMP with DNA-PKcs

in these conditions (Figure 1C). Similarly, when endogenous DNA-PKcs was immunoprecipitated (Figure S1A), the presence of DNA-PKcs in immunoprecipitates (Figure S1B) correlated with detection of 2'3'-cGAMP following *in vitro* binding assays (Figure S1C). To further exclude the contribution of DNA-PKcs co-factors in the binding to 2'3'-cGAMP, we performed similar experiments using recombinant DNA-PKcs (Figure 1D and Figure S1D). We found a significant enrichment of 2'3'-cGAMP, when recombinant DNA-PKcs was immunoprecipitated (Figure 1E). Conversely, we conducted experiments where FLAG-immunoprecipitated FLAG-DNA-PKcs was peptide-eluted under native conditions prior to incubation with Streptavidin beads-immobilized biotinylated 2'3'-cGAMP or biotin (Figure 1F). Western blot analyses showed enrichment of DNA-PKcs with biotinylated 2'3'-cGAMP (Figure 1G). Immunofluorescence analyses also showed co-localization between DNA-PKcs and 2'3'-cGAMP (Figure 1 H-I). Thermal shift assays (TSA) were then conducted using either using whole cell lysates (Figure 1J-K and Figure S1E-F), or FLAG-purified FLAG-DNA-PKcs (Figure 1L-M). Incubation with 2'3'-cGAMP led to stabilization of DNA-PKcs both in whole cell extracts (Figure 1K, Table I) and immunoprecipitates (Figure 1M). TSA performed using the NU7441 DNA-PKcs competitive inhibitor (Leahy et al., 2004) showed selective stabilization of DNA-PKcs but not of STING (Figure S1E-F).

Taken together, these data show that DNA-PKcs physically interacts with 2'3'-cGAMP.

2'3'-cGAMP interacts with the catalytic site of DNA-PKcs

We next aimed to identify the domain of DNA-PKcs interacting with 2'3'-cGAMP. We first performed molecular modelling and docking analyses to identify putative binding regions. We used the resolved crystal of human DNA-PKcs (RCBS: 5LUQ) for docking experiments using 2'3'-cGAMP. This predicted that 2'3'-cGAMP can dock into DNA-PKcs catalytic pocket (Figure 1N and Figure S1G-H), adopting a stable conformation (Energy -28940.5Kcal/mol, Table II), notably through strong H-bonds between DNA-PKcs residues Asp3723, Arg3741, His1069 and Asp3744, Arg3746, His3748 with the phosphodiester bonds within the 2'3'-cGAMP molecule (Figure S1I-J). To control for specificity we used other DNA repair-related enzymes belonging to the phosphatidylinositide 3-kinase (PI3K)-related kinase family, to which DNA-PKcs belongs, namely Ataxia Telangiectasia Mutated (ATM; 8OXQ) and Ataxia Telangiectasia and Rad3-related protein (ATR; 5YZ0), which possess analogous catalytic sites competent for ATP binding and hydrolysis. The available structures of ATM and ATR were superposed with that of DNA-PKcs, and comparative analysis of their catalytic cleft predicted that 2'3'-cGAMP is unlikely to interact with these catalytic domains (Figure S1K-L). Altogether, these *in silico* data suggest selective interaction of 2'3'-cGAMP with DNA-PKcs in its catalytic pocket.

We reasoned that if 2'3'-cGAMP interacts with DNA-PKcs catalytic pocket, it could be expected to reduce DNA-PKcs ability to hydrolyze ATP. We thus used an *in vitro* assay to measure the kinase activity of DNA-PKcs in the presence of increasing doses of 2'3'-cGAMP. The NU7441 competitive DNA-PKcs inhibitor was used as a positive control. Increasing 2'3'-cGAMP concentration led to inhibition of DNA-PKcs catalytic activity in a dose-dependent manner (Figure 1O), supporting binding of 2'3'-cGAMP in the catalytic cleft of DNA-PKcs. We next used recombinant DNA-PKcs for *in vitro* 2'3'-cGAMP binding assays, in which NU7441 was used as a competitor. NU7441 displaced the interaction of 2'3'-cGAMP with DNA-PKcs (Figure 1P and S1M-N), suggesting that the interaction of 2'3'-cGAMP with DNA-PKcs occurs in its catalytic cleft.

To confirm that the interaction of 2'3'-cGAMP with DNA-PKcs occurs in the catalytic domain, we generated DNA-PKcs mutants where the kinase domain is deleted (FLAG-DNA-PKcs-ΔK) or corresponding to the kinase domain alone (FLAG-Kinase). Thermal shift assays were conducted on full-length and truncations mutants of DNA-PKcs, showing that 2'3'-cGAMP stabilized both FLAG-DNA-PKcs and FLAG-Kinase, but not FLAG-DNA-PKcs-ΔK (Figure 1Q). Binding assays were then performed using full-length and DNA-PKcs truncations. Full-length FLAG-DNA-PKcs and FLAG-DNA-PKcs-Kinase both interacted with 2'3'-cGAMP while FLAG-DNA-PKcs-ΔK was not retrieved in the pulldown assay (Figure 1R).

Altogether, our data show that DNA-PKcs interacts directly with 2-3'-cGAMP through its catalytic domain.

DNA-PK regulates 2'3-cGAMP-associated STING signaling

Interaction of 2'3'-cGAMP with DNA-PKcs may affect 2'3'-cGAMP biological activity. We thus assessed the impact of DNA-PKcs on 2'3'-cGAMP-associated signaling.

To this aim, we treated T98G cells with 2'3'-cGAMP in the presence or absence of NU7441 and analyzed STING activation. Of note, T98G cells do not express detectable levels of cGAS and are therefore a good model to study the direct effect of DNA-PKcs on 2'3'-cGAMP excluding confounding effects associated with the role of DNA-PKcs as a co-activator of cGAS (Taffoni et al., 2023). Expectedly, 2'3'-cGAMP treatment alone led to STING degradation, STING phosphorylation (pSTING), and IRF3 phosphorylation (Figure 2A), accompanied by upregulation of *IFNB1* expression (Figure 2B). Attesting to the production of bioactive IFNs, increased expression of the *ISG15*, *IFIT1*, and *CCL5* interferon-stimulated genes (ISGs) was measured following 2'3'-cGAMP treatment (Figure 2B). Combining 2'3'-cGAMP treatment with NU7441-mediated DNA-PKcs inhibition led to increased pSTING and pIRF3 levels (Figure 2A,

compare lanes 2 and 4) and enhanced the expression of *IFNB1*, *ISG15*, *IFIT1*, and *CCL5* (Figure 2B) when compared to treatment with 2'3'-cGAMP alone. The induction of type I IFN responses is also observed upon measurement of produced IFNβ (Figure 2C), CXCL10 and CCL5 (Figure S2A). Similar results were obtained with a panel of DNA-PKcs inhibitors (Figure S2B), confirming that DNA-PKcs inhibition is associated with boosted 2'3'-cGAMP signaling. This is in contrast to what is observed when T98G cells stably expressing cGAS (T98G^{cGas}) are challenged with dsDNAs, which results in decreased *IFNB1*, *CXCL10* and *IFIT2* expression (Figure S2C).

To confirm a direct role of DNA-PKcs in inhibition of 2'3'-cGAMP signaling, we next used small interfering RNAs (siRNAs) targeting DNA-PKcs or KU70 (Figure S2D). Treatment with 2'3'-cGAMP following knock-down of DNA-PKcs, but not of KU70, increased expression of STING-associated transcripts such as *IFNB1*, *ISG15*, *CXCL10*, and *IFIT2* (Figure 2D), phenocopying the effect of NU7441 treatment. Similarly, we found that in DNA-PKcs knockout cells (Figure S2E), 2'3'-cGAMP-associated type I IFN signaling was boosted (Figure 2E). Thus, DNA-PKcs inhibition or ablation enhances 2'3'-cGAMP-associated type I IFN responses.

We next sought to verify if DNA-PKcs-mediated type I IFN signaling relies on the canonical STING-dependent pathway. To this aim, we used THP-1 human myeloid cell lines knocked-out for cGAS (THP-1$^{cGAS-/-}$) or STING (THP-1$^{STING-/-}$) and isogenic control cells (THP-1^{CTRL}). Cells were mock-treated or treated with 2'3'-cGAMP and NU7441 individually or in combination. Gene expression and WB analyses showed that combining 2'3'-cGAMP treatment with DNA-PKcs inhibition boosted the activation of STING-dependent signaling in THP-1^{CTRL} and THP-1$^{cGAS-/-}$, resulting in increased phosphorylation of IRF3 and STING (Figure S2F-H) and increased expression of *IFNB1*, *CXCL10*, *ISG15*, and *IFIT2* (Figure 2F). However, in STING-deficient THP-1 cells, the 2'3'-cGAMP-associated response was abrogated, regardless of NU7441 treatment (Figure 2F and Figure S2F-H 2E). This pattern is also reflected at the cytokine production level (Figure 2G and S2I). To confirm that the observed increase in type I IFN responses upon combining 2'3'-cGAMP stimulation and DNA-PKcs inhibition, we performed similar experiments in THP-1 cells expressing a DNA-PKcs-targeting guide RNA (Figure 2F and Figure S2J). Similar results were obtained in T98G cells knocked-out for STING (T98G$^{STING-/-}$) (Figure S2K-L). In T98G cells knocked-out for the Interferon-α/β receptor (IFNAR), combining DNA-PKcs inhibition with 2'3'-cGAMP boosted hallmarks of STING activation (Figure S2M). Thus, DNA-PKcs-mediated inhibition of 2'3'-cGAMP signaling is independent of cGAS, requires the presence of STING, but is not a consequence of IFNAR-dependent signaling.

We next asked how DNA-PKcs-mediated 2'3'-cGAMP inhibition impacts on dsDNA-associated signaling. To this aim, T98G^{cGAS} were transfected or not with dsDNA for up to 48 hours, in the presence or absence of NU7441. As expected, gene expression analyses showed that DNA-PKcs inhibition impaired dsDNA-associated type I IFN responses at early time points (up to 6 hours; Figure 2I). However, this phenotype was reverted at later time points (from 16 to 48 hours; Figure 2I). Proteome profiler analyses were conducted at 24 hours post-stimulation with dsDNA in the presence or absence of NU7441, showing that DNA-PKcs inhibition enhanced the production of numerous cytokines and chemokines (Figure 2J). Similar experiments were performed in THP-1 cells, where we found that NU7441 treatment, in combination with dsDNA transfection led to decreased type I IFN responses at early time points (3-6 hours; Figure S2N) and boosted type I IFN responses at later time points (16-24 hours; Figure S2N). The net inflammatory output resulted in DNA-PKcs inhibition enhancing the production of cytokines and chemokines (Figure S2O).

Finally, human STING haplotypes deficient for optimal type I IFN response induction have been reported (Aybar-Torres et al., 2024, Simchoni et al., 2025, Yi et al., 2013). We questioned whether DNA-PKcs inhibition may alter their response threshold to 2'3'-cGAMP stimulation. STING knockout THP-1 cells were engineered to express human STING haplotypes (STING-H232, STING-AQ and STING-HAQ), prior to DNA-PKcs inhibition and 2'3'-cGAMP stimulation. We found that DNA-PKcs inhibition led to increased 2'3'-cGAMP activation of type I IFN responses in cells expressing STING-HAQand STING-AQ, but not STING-H232 (Figure S2P). Interestingly, as observed in Figure S2K, DNA-PKcs inhibition led to decreased dsDNA induced Stimulation of Type I IFN responses (Figure S2Q).

Together, our data establish that DNA-PKcs inhibits 2'3'-cGAMP signaling, thereby contributing to signal termination following activation of the cGAS-STING axis.

DNA-PKcs regulates the activity of 3'3'-cGAMP

Mammalian regulators of 2'3'-cGAMP have been shown to operate selectively on 2'3'-cGAMP (Hou et al., 2023, Li et al., 2014, Mardjuki et al., 2024). We thus questioned the spectrum of DNA-PKcs activity on CDNs.

We assessed the capacity of DNA-PKcs to inhibit CDNs of bacterial origin: 3'3'-cGAMP (Zhang et al., 2013), bis-(3'-5')-cyclic dimeric adenosine monophosphate (c-di-AMP), and bis-(3'-5')-cyclic dimeric guanosine monophosphate (c-di-GMP) (Burdette et al., 2011, Jin et al., 2011). We assessed the impact of these CDNs on DNA-PKcs catalytic activity *in vitro*. We found that 3'3'-cGAMP, but not c-di-AMP nor c-di-GMP, inhibited DNA-PKcs (Figure 3A and Figure S3A).

Docking analyses supported that 3'3'-cGAMP, but not c-di-AMP nor c-di-GMP, can interact with DNA-PKcs in its catalytic cleft adopting a stable conformation (Energy -29962.4 Kcal/mol, Table II). We also observed that recombinant DNA-PKcs interacts with 3'3'-cGAMP but not with c-di-AMP (Figure 3B).

To test whether the interaction between DNA-PKcs and 3'3'-cGAMP translates into signaling inhibition, we treated THP-1 and T98G cells with 3'3'-cGAMP alone or in combination with NU7441. Combining 3'3'-cGAMP treatment with DNA-PKcs inhibition enhanced STING phosphorylation (Figure 3C and Figure S3B) and increased expression of STING activity-associated transcripts such as *IFNB1*, *ISG15*, *IFIT1*, and *CCL5* in both cell types (Figure 3D and Figure S3C) when compared to cells treated only with 3'3'-cGAMP. We also measured increased production of IFNβ, CXCL10 and CCL5 when 3'3'-cGAMP and NU7441 treatments were combined in THP-1 cells (Figure 3E). To confirm that this effect is directly mediated by DNA-PKcs we performed 3'3'-cGAMP treatment in THP-1^{CTRL} and THP-1$^{gDNA\text{-}PKcs}$. We observed that Type I IFN responses were potentiated in THP-1$^{gDNA\text{-}PKcs}$ as compared to control cells (Figure 3F). Similar experiments were next conducted on human primary macrophages (Figure S3 D-E). Gene expression analyses showed that combining NU7441 with 3'3'-cGAMP treatment boosted *IFNB*, *ISG15, IFIT1*, and *CCL5* expression (Figure 3G and Figure S3F) when compared to 3'3'-cGAMP alone. Thus, the negative regulatory role of DNA-PKcs on 3'3'-cGAMP bioactivity can also be measured in primary human cells.

Combined, our data show that DNA-PKcs selectively interacts with 3'3'-cGAMP to inhibit STING-dependent signaling in immune and non-immune cells, but does not interfere with other tested bacterial CDNs.

DNA-PKcs selectively inhibits the activity of STING-targeting drugs

STING is an important biomedical drug target for which a plethora of small molecule agonists are in clinical trials (Hines et al., 2023). We questioned whether DNA-PKcs may interact with these compounds, and impact their potency.

We first performed DNA-PKcs activity assays in the presence of increasing doses of two STING agonists, E7766 and ADU-S100. E7766, but not ADU-S100, inhibited DNA-PKcs activity (Figure 3H), suggesting interaction of E7766 with DNA-PKcs catalytic domain. Functional assessment of the impact of DNA-PKcs on the activity of these compounds was tested by treating cells with E7766 or ADU-S100 in combination with NU7441 or not. DNA-PKcs inhibition boosted type I IFN responses when combined with E7766 (Figure 3I and Figure S3G) but not with ADU-S100 (Figure 3J and Figure S3H). These data were supported by *in*

silico docking analyses that showed that E7766 presents a strong capacity to interact with DNA-PKcs, as compared to ADU-S100 (Table II).

Additional experiments were conducted using the diABZI STING agonist, showing that combination with NU7441 potentiated type I IFN responses (Figure 3K and Figure S3I). Similar to what was observed for 2'3'-cGAMP and 3'3'-cGAMP, we found that treatment of THP-1$^{gDNA-PKcs}$ with E7766 and diABZI led to enhancement of type I IFN responses when compared to control cells (Figure S3J-K).

These data thus show that DNA-PKcs inhibition selectively alters the potency of STING agonists.

DNA-PKcs regulates the activity of STING agonists in vivo

We next sought to assess whether the inhibitory effect of DNA-PKcs on STING agonists is recapitulated *in vivo*. Conflicting data were reported concerning the capacity of DNA-PKcs to act as a cytosolic dsDNA sensor in murine cells (Ferguson et al., 2012, Burleigh et al., 2020), warranting assessment of the inhibitory role of DNA-PKcs on 2'3'-cGAMP in murine models. We thus evaluated the impact of combining NU7441 with diABZI or E7766 on STING-dependent signaling in the RAW264.7 myeloid murine cell line. Similar to what we observed in human cell lines, the combination of DNA-PK inhibition with STING agonists boosted the expression of *Interferon β* (*Ifnβ*), as well as of the *Isg15*, *Ifit1*, *Ccl5* and *Cxcl10* ISGs (Figure 4A and Figure S4A). We next isolated primary splenocytes from mice and assessed the impact of combining 3'3'-cGAMP or diABZI with NU7441 (Figure 4B). We found that combining NU7441 with 3'3'-cGAMP boosted inflammatory gene expression (Figure 4C) as well as cytokine production (Figure 4D-E). Similarly, co-treatment with NU7441 and diABZI boosted expression and production of inflammatory cytokines (Figure 4F-G). Thus, DNA-PKcs inhibits CDN-associated signaling in murine cells.

Sting-deficient (*Sting-/-*), Ifnar-deficient (*Ifnar-/-*) mice and WT littermates were subjected or not to intraperitoneal injections of NU7441, prior to injection of diABZI followed by analysis of hallmarks of STING activation in peritoneal fluids, peritoneal macrophages, peritoneum and spleens (Figure 4I). Gene expression analyses showed that combining DNA-PK inhibition with STING agonist boosted the expression of transcripts associated with STING signaling in the peritoneum (Figure 4J) peritoneal macrophages (Figure 4K), and the spleen (Figure 4L), accompanied by enhanced Cxcl10 production in the peritoneal fluid and in the spleen (Figure 4M-N). Interferon response genes were not increased in any of the tested conditions in Sting-deficient mice (Figure 4J-N), supporting that DNA-PK-dependent regulation of type I IFN

responses relies on Sting. Absence of upregulation in Ifnar-deficient mice supports that in WT mice (Figure 4J-N), bioactive interferons are produced to stimulate the expression of tested ISGs.

Altogether, these data demonstrate DNA-PKcs inhibits agonist-dependent STING signaling *in vivo*.

DNA-PKcs-associated CDN signaling inhibition regulates the establishment of an antiviral state

We next asked whether the negative role of DNA-PKcs on STING agonists translates into a biologically relevant functional response. We therefore assessed the impact of DNA-PKcs inhibition on the establishment of an antiviral state. We used two DNA viruses, namely the herpes simplex virus 1 (HSV-1) and Monkey Pox virus (MPXV), and one RNA virus, the vesicular stomatitis virus (VSV), all of which are sensitive to IFN responses.

We treated T98G cells with 3'3'-cGAMP, diABZI and E7766 STING agonists, individually or in combination with NU7441, prior to infection with the 3 aforementioned viruses and measurement of the percentage of infected cells (Figure 5A). As expected, treatment with STING agonists alone was sufficient to decrease infection by HSV-1 (Figure 5B-C), MPXV (Figure 5D and Figure S5A) and VSV (Figure 5E and Figure S5B). Combining STING agonists with NU7441 further decreased viral infection (Figure 5B-E and Figure S5A-B). Dependency on DNA-PKcs for this phenotype was confirmed using DNA-PKcs deficient cells (Figure S5C). Of note, treatment with the NU7441 alone increased infection, which likely reflects a direct antiviral role of DNA-PKcs.

We next assessed the impact of DNA-PKcs antagonism on the STING agonist-induced antiviral status in human primary cells. Human primary macrophages (Figure S5D) were treated with NU7441 in combination or not with STING agonists prior to infection with VSV. As observed in T98G cells, combining DNA-PKcs inhibition with STING agonism increased the inhibition of infection with VSV (Figure 5F-G, Figure S5E-F). Thus, combining STING activation and DNA-PK inhibition promotes the establishment of a higher antiviral state, supporting the role of DNA-PKcs in the negative regulation of STING agonists.

Finally, we investigated the contribution of DNA-PKcs in the resolution of virus-induced inflammatory responses. To this aim, mouse embryonic fibroblasts were infected with HSV-1 in the presence of NU7441 ('pre-treatment') or treated with NU7441 6 hours post infection ('post-treatment'), prior to gene expression analyses (Figure 5H). Gene expression analyses

showed that while DNA-PKcs inhibition during HSV-1 infection led to decreased inflammatory responses (Figure 5I), treatment with NU7441 6 hours post-infection led to increased inflammatory gene expression (Figure 5I). This suggests that during early steps of infection (pre-treatment), DNA-PKcs is antiviral, while at later steps it plays a pro-viral role. These data further support a role of DNA-PKcs in the resolution of 2'3'-cGAMP signaling.

Together, these data show that DNA-PKcs is a regulator of STING-dependent antiviral responses in cell lines and primary human cells, likely through the control of 2'3'-cGAMP. This supports that in addition to previously reported roles of DNA-PKcs in activating type I IFN resposens alongside the cGAS-STING pathway, DNA-PKcs buffers STING overactivation through the trapping of 2'3'-cGAMP.

Discussion

We describe a conserved function of DNA-PKcs in the regulation of 2'3'-cGAMP and 3'3'-cGAMP CDNs-associated inflammatory responses. We show that DNA-PKcs binds to those CDNs selectively, decreasing their availability for interaction with STING and thereby buffering their activity. This is complementary to other mechanisms described to control CDN activity through extracellular 2'3'-cGAMP levels (Hou et al., 2023, Li et al., 2014, Mardjuki et al., 2024). That DNA-PKcs also ensures termination of 3'3'-cGAMP-associated inflammatory responses appears as a distinctive feature and may have evolved as a defense mechanism towards 3'3'-cGAMP-producing pathogenic bacteria (Davies et al., 2012). Since DNA-PKcs is highly conserved in the tree-of-life (Lees-Miller et al., 2021), one may question whether this mechanism operates as a general mechanism to prevent overactivation of inflammatory responses in response to pathogen infection.

Conflicting reports exist in the literature, opposing a pro- and anti-inflammatory role of DNA-PKcs in nucleic acid immunity (Burleigh et al., 2020, Hristova et al., 2024, Taffoni et al., 2023, Sun et al., 2020). Our work reconciles these prior studies, showing that DNA-PK is indeed involved as a detector of incoming DNA viruses, that potentializes the initial activation of type I IFN responses (Burleigh et al., 2020, Ferguson et al., 2012, Taffoni et al., 2023), but also inhibits CDN to ensure signal termination. Combined the current evidence therefore suggests that DNA-PK has a dual role in modulating cGAS-STING signaling, regulating the amplitude and kinetics of dsDNA responses, as well as homeostatic inflammation, ultimately decreasing overall signaling output. Early upon exposure of dsDNA species in the cytosol, DNA-PK senses incoming DNA in parallel of the cGAS-STING pathway (Burleigh et al., 2020, Ferguson et al., 2012, Taffoni et al., 2023)and catalyses activating phosphorylation of cGAS (Taffoni et al., 2023), while excess of produced 2'3'-cGAMP is trapped by DNA-PKcs to prevent

overactivation of STING. This fits with a multifunctional roles of DNA-PK, in the regulation of inflammatory responses (Wu et al., 2024).

We also demonstrate that 2’3’-cGAMP and 3’3’-cGAMP block DNA-PKcs catalytic activity, which may have an impact on its ability to repair double-strand breaks. However, previous studies have shown that the levels of DNA-PK do not correlate with DNA repair functions (Meek et al., 2008) and that other pathways can take over non-homologous end-joining (NHEJ)-mediated repair when DNA-PKcs is non-functional (Blackford and Jackson, 2017). Disentangling the relative contribution of DNA-PK repair function and regulation of inflammatory responses is therefore a difficult task. It is however possible to speculate that CDN-mediated DNA-PKcs inhibition may have a distinct impact on specific repair functions, such as in micronuclei damage (Harding et al., 2017) or immunoglobulin class switching (Bjorkman et al., 2015), which are contexts where DNA-PK inhibition would impact immune function. This further suggests potential cell-type specific roles of DNA-PKcs signaling functions. In addition, owing to the abundance of DNA-PKcs, the small percentage of the protein sufficient for repair function and functional redundancy of repair pathways, it has been previously speculated that DNA-PKcs role beyond DNA repair may be its most prominent function (Taffoni et al., 2021, Wu et al., 2024). How CDN-mediated inhibition of DNA-PK impacts those other DNA-PKcs functions would require further investigations.

The ability of DNA-PKcs to control CDN-associated inflammatory responses is relevant for drugs designed to activate STING in immunosuppressed contexts such as the tumor microenvironment. Existing STING agonists have distinct features. Amongst tested compounds in the present study, ADU-S100, E7766 and diABZi all present the ability to interact with the STING CDN-binding domain. ADU-S100 is a synthetic CDN STING agonist, structurally similar to c-diAMP (Corrales et al., 2015), and both compounds present a poor capacity to interact with DNA-PKcs. In contrast, E7766 and diABZI that are macrocycle-bridged and non-nucleotide-based STING agonists (Huang et al., 2022) were found to have their bioactivity regulated by DNA-PKcs, suggestive of interaction with DNA-PKcs. Precise assessment of the contact points of STING agonists with the catalytic cleft of DNA-PKcs is warranted in order to fully evaluate what explains these discintive features. Furthermore, whether the capacity of these compounds to interact with DNA-PKcs correlates with DNA repair deficiency-associated side-effects remains to be assessed. Thus, the status of DNA-PKcs in target tissues may be important to allow prediction of the capacity of STING agonists to induce beneficial inflammation. For instance, in the context of cancer immunotherapy where STING agonists are used to boost inflammatory responses (Hines et al., 2023), the presence of DNA-PKcs anomalies, such as frequent copy number variations (Yang et al., 2020) must be

assessed. It is therefore important to take into account the status of DNA-PKcs in patients enrolled in STING-agonist-based clinical trials for better stratification.

Limitations of the study

Further work will be required to demonstrate the impact of DNA-PKcs inhibition in the context of cancer. The risks associated with DNA-PK-mediated DNA repair impairment should also be assessed in order to evaluate the full impact on anti-tumoral responses. In addition, DNA-PKcs has been reported to be involved in B cells Immunoglobulin class switching (Bjorkman et al., 2015). Although alternative routes to non-homologous end-joining may be used to ensure IgG class switching, the impact on B cell development and functionality must be assessed formally. Finally, we identify that CDNs bind into the catalytic pocket of DNA-PKcs. Point mutations may allow the identification of precise contact points and allow for rationalized drug design of STING agonists that do not impede DNA-PKcs catalytic activity.

Tables

Table I. Stabilization of DNA-PKcs in the presence of 2’3’-cGAMP. Ratio of DNA-PKcs over HSP90 protein intensity.

Temperature (C°)	46.9	49.5	52.0	54.5	57.1	59.3	60.9	61.7
Mock	1.0	0.8	0.8	0.7	0.5	0.4	0.4	0.4
2’3’-cGAMP	1.0	1.1	1.3	1	0.6	0.5	0.5	0.5

Table II. Energies of interaction of DNA-PKcs with E7766, ADU-S100, 2’3’-cGAMP and 3’3’-cGAMP. ALL: complex energy; INT: interaction energy; VDW: Van der Waals. Calculated energies are expressed in kcal.mol^{-1}.

		Energy	strain	vdw	Electrostatic
E7766	ALL:	-30117.9	1047.319	6185.434	-38134.0
	INT:	-356.591	0.000	-34.800	-321.791
3’3’cGAMP	ALL:	-29962.4	1144.894	6179.537	-38141.1
	INT:	-237.989	0.000	-44.032	-193.956
2’3’cGAMP	ALL:	-28940.5	1386.534	6972.405	-38159.4
	INT:	-172.032	0.000	34.283	-206.314
ADU-S100	ALL:	-28640.3	1469.651	7567.148	-38477.2
	INT:	932.682	0.000	1321.216	-388.534

Figure Legends

Figure 1. 2'3'-cGAMP interacts with the catalytic pocket of DNA-PKcs.

(A). Experimental Scheme for **B** and **C**. FLAG-tagged DNA-PKcs (FLAG-DNA-PKcs) expressed in 293T cells was FLAG immunoprecipitation (IP), prior to incubation with 2'3-cGAMP, release of bound 2'3'-cGAMP and detection by ELISA**.**

(B) Western blot (WB) analysis of Input and FLAG-IP performed as in **A** was conducted using the indicated antibodies. **Representative WB of 3 independent experiments**.

(C) 2'3'-cGAMP was measured by ELISA on experiment performed as in **A**. Graph presents the mean ± standard error from the mean (SEM) of 3 independent experiments. Statistical significance was calculated by 2-tailed Student T-test.

(D) Experimental scheme for **E**. Recombinant DNA-PKcs was immunoprecipitated using a DNA-PKcs-specific antibody, prior to incubation with 2'3'-cGAMP, release of bound 2'3'-cGAMP, and detection by ELISA.

(E) Graph represents mean (±SEM) 2'3'-cGAMP levels as measured in Mock IgG and DNA-PK-specific IP performed as in **D**. Statistical significance was calculated by 2-tailed Student T-test. **n=3 independent experiments.**

(F) Experimental Scheme for **G**. FLAG-tagged DNA-PKcs (FLAG-DNA-PKcs) expressed in 293T cells was FLAG-purified prior to incubation with biotin or biotinylated 2'3'-cGAMP (C3-2'3'-cGAMP), followed by streptavidin pull-down, and WB analysis.

(G) WB analysis of Input and streptavidin pull-down experiment performed as in **F** was performed using a FLAG-specific antibody. **Representative WB of 3 independent experiments**.

(H) DNA-PKcs (red) and 2'3'-cGAMP (green) subcellular localization was assessed 6 hours post iFluor488-2'3'-cGAMP transfection in T98G cells. Immunofluorescence was performed using a DNA-PKcs-specific antibody and DAPI nuclear staining. Representative images of 15-20 images, Scale bars 5µM.

(I) Quantification of cytosolic DNA-PKcs and iFluor488-2'3'-cGAMP foci colocalization following transfection of T98G cells with mock or fluorescent 2'3'-cGAMP using CellProfiler software. n = 424 and 558. Statistical significance was calculated by 2-tailed Student T-test.

(J) Experimental scheme for K. THP-1 cells were processed for thermal shift assay (TSA) in the presence or absence of 2'3'-cGAMP.

(K) WB analysis of TSA, as described in **J,** was conducted using indicated antibodies. **Representative WB of 3 independent experiments**.

(L) Experimental Scheme for **M**. purified FLAG-DNA-PKcs was used as input material for TSA in the presence or absence of 2'3'-cGAMP.

(M) WB analysis of TSA, performed as in **L,** was conducted using anti-FLAG antibody**.** **Representative WB of 3 independent experiments**.

(N) Representation of the molecular modeling of 2'3'-cGAMP in interaction with DNA-PKcs.

(O) ATP hydrolysis by DNA-PK was measured in vitro in presence of NU7441 or increasing doses 300µM-2700µM of 2'3'-cGAMP. Graph presents the mean of 3 independent experiments. One-way ANOVA.

(P) As in D, except that DNA-PKcs IP was incubated with or without 2'3'-cGAMP in presence or not of NU7441 inhibitor (used as a competitor) prior to measurement of bound 2'3'-cGAMP**.** Graph represents mean (±SEM) 2'3'-cGAMP levels, **n=3 independent experiments**. Statistical significance was calculated by 2-tailed Student T-test**.**

(Q) FLAG-DNA-PKcs, FLAG-DNA-PKcs-Δkinase and FLAG-Kinase were expressed in 293T cells prior to TSA analysis in the presence or absence of 2'3'-cGAMP. WB was conducted with the indicated antibodies. **Representative WB of 3 independent experiments**.

(R) FLAG-DNA-PKcs, FLAG-DNA-PKcs-Δkinase and FLAG-Kinase were FLAG purified as in A prior to incubation with biotin or biotinylated 2'3'-cGAMP as in I. WB analysis was conducted using FLAG antibody. **Representative WB of 3 independent experiments**.

****: $p<0.0001$; ***: $p<0.001$; **: $p<0.01$; *: $p<0.05$; ns: not significant.

Also see Figure S1.

Figure 2. DNA-PKcs dampens 2'3'cGAMP signaling

(A) T98G cells were treated or not with 2µM NU7441 DNA-PKcs inhibitor for 1 hour prior to transfection or not of 10µg/ml 2'3'-cGAMP for 6 hours and analysis of WCE by WB using indicated antibodies. **Representative WB of 3 independent experiments**.

(B) As in **A**, except that gene expression analysis was conducted. Graphs represent mean (±SEM), **n=3 independent experiments**. Statistical significance was calculated by 2-tailed Student T-test.

(C) As in **A**, except that IFNβ levels were measured by ELISA 6 hours post treatment. Graphs represent mean (±SEM), **n=3 independent experiments**. Statistical significance was calculated by 2-tailed Student T-test.

(D) T98G cells were transfected for DNA-PKcs- or KU70-targeting siRNA or a control non targeting siRNA prior to transfection or not of 2'3'-cGAMP for 6 hours and gene expression analyses. Graphs represent mean (±SEM), **n=3 independent experiments**. Statistical significance was calculated by 2-tailed Student T-test.

(E) Control and DNA-PKcs knockout T98G cells were transfected with 2'3'cGAMP for 6 hours prior to gene expression analysis. Graphs present mean (±SEM), **n=3 independent experiments**. Statistical significance was calculated by 2-tailed Student T-test.

(F) Control (CTRL), cGAS-/- and STING-/- THP-1 cells were treated or not with 2µM of NU7441 for 1 hour prior to transfection of not with 10µg/ml 2'3'-cGAMP for 6 hours and gene expression analysis. Graphs present mean (±SEM), **n=3 independent experiments**. Statistical significance was calculated by 2-tailed Student T-test.

(G) As in **F**, except that CXCL10 levels were measured by ELISA 6 hours post treatment. Graphs represent mean (±SEM), **n=3 independent experiments**. Statistical significance was calculated by 2-tailed Student T-test.

(H) Control and DNA-PKcs knockout THP-1 cells were transfected with 2'3'cGAMP for 6 hours prior to gene expression analysis. Graphs present mean (±SEM), **n=3 independent experiments**. Statistical significance was calculated by 2-tailed Student T-test.

(I) T98G expressing cGAS ($T98G^{cGAS}$) were transfected with dsDNA in presence or absence of NU7441. Gene expression analysis was conducted at 3, 6, 16, 24 and 48 hours post transfection. Graphs present mean (±SEM) **of 3 independent experiment**. Statistical significance was calculated by 2-tailed Student T-test.

(J) $T98G^{cGAS}$ were transfected or not with dsDNA in presence or absence of NU7441 for 24 hours prior to analysis of cytokines in media using cytokine arrays. Heatmap (representative of n=2 independent experiments) represents fold change spot intensity in NU7441-treated samples versus vehicle.

****: $p<0.0001$; ***: $p<0.001$; **: $p<0.01$; *: $p<0.05$; ns: not significant.

Also see Figure S2.

Figure 3. DNA-PKcs inhibits 3'3'-cGAMP- and agonist-associated STING activation.

(A) ATP hydrolysis by DNA-PK was measured *in vitro* in presence of increasing doses (0.8 µM to 2500 µM) of 3'3'-cGAMP or c-di-AMP. Graph presents the mean of 3 independent experiments. Statistical significance was calculated by one-way ANOVA.

(B) Recombinant DNA-PKcs was immunoprecipitated using either mock IgG to a DNA-PKcs-specific antibody prior to incubation with 3'3'-cGAMP or c-di-AMP and ELISA-based measurement of bound CDNs. Graph presents mean (±SEM) 3'3'-cGAMP and c-diAMP levels as measured in Mock and DNA-PKcs-specific IP in 3 independent experiments. Statistical significance was calculated by 2-tailed Student T-test.

(C) THP-1 cells were treated or not with 2 µM NU7441 in combination or not with 10µg/ml fluorinated 3'3'-cGAMP for 6 hours prior to WB analysis using the indicated antibodies. **Representative WB of 3 independent experiments**.

(D) As in **C**, except that gene expression analyses were conducted. Graphs present the mean (±SEM) of 3 independent experiments. Statistical significance was calculated by 2-tailed Student T-test.

(E) As in **C**, except that IFNβ, CXCL10 and CCL5 levels were measured by ELISA. Graphs present the mean (±SEM) of 3 independent experiments. Statistical significance was calculated by 2-tailed Student T-test.

(F) Control and DNA-PKcs knockout THP-1 cells were treated with 3'3'cGAMP for 6 hours prior to gene expression analysis. Graphs present mean (±SEM), **n=3 independent experiments**. Statistical significance was calculated by 2-tailed Student T-test.

(G) Human primary monocytes were isolated from buffy coats prior to treatment or not with 2µM NU7441 for 1 hour followed by administration of 10µg/ml fluorinated 3'3'-cGAMP for 6 hours and gene expression analysis. Graphs present the mean (±SEM) of 3 independent experiments. Statistical significance was calculated by 2-tailed Student T-test.

(H) ATP hydrolysis by DNA-PK was measured *in vitro* in presence of increasing doses (0.8 µM to 2500 µM) of E7766 or ADU-S100. Statistical significance was calculated by one-way ANOVA.

(I) T98G cells were treated or not with 2µM of NU7441 prior to addition or not of 1 µM of E7766 STING agonist for 3 hours and gene expression analysis. Graphs present the mean (±SEM), **n=3 independent experiments**. Statistical significance was calculated by 2-tailed Student T-test.

(J) T98G cells were treated or not with 2µM of NU7441 prior to addition or not of 50 µM of ADU-S100 STING agonist for 3 hours and gene expression analysis. Graphs present the mean

(±SEM), **n=3 independent experiments**. Statistical significance was calculated by 2-tailed Student T-test.

(K) T98G cells were treated or not with 2µM of NU7441 prior to addition or not of 10 µM of diABZI for 3 hours and gene expression analysis. Graphs present the mean (±SEM), **n=3 independent experiments**. Statistical significance was calculated by 2-tailed Student T-test.

****: $p<0.0001$; ***: $p<0.001$; **: $p<0.01$; *: $p<0.05$; ns: not significant.

Also see Figure S3

Figure 4. DNA-PKcs inhibits STING agonists-induced inflammatory responses in murine models.

(A) RAW264.7 cells were treated or not with NU7441 1h before stimulation with 10µM diABZI or 1µM E7766) for 6h prior to gene expression analyses. Graphs present the mean (±SEM) of 3 independent experiments. Statistical significance was calculated by One-way ANOVA with multiple comparison.

(B) Experimental scheme: Spleens were harvested from 8 mice, primary splenocytes isolated and treated with NU7441 for 6h with 3'3'-cGAMP or diABZI, prior to gene expression analysis and cytokine measurement.

(C) Gene expression analysis was conducted on primary cells treated as described in B with 3'3'-cGAMP. Graphs present the mean (±SEM) of 3 independent experiments. Statistical significance was calculated by 2-tailed Student T-test.

(D) Heatmap presents cytokines that were measured in the supernatant of cells from C.

(E) Mean centroid analysis of cytokines presented in D. Statistical significance was calculated by 2-tailed Student T-test.

(F) Gene expression analysis was conducted on primary cells treated as described in B with diABZI. Graphs present the mean (±SEM) of 3 independent experiments. Statistical significance was calculated by 2-tailed Student T-test.

(G) Heatmap presents cytokines that were measured in the supernatant of cells from F.

(H) Mean centroid analysis of cytokines presented in G. Statistical significance was calculated by 2-tailed Student T-test.

(I) *In vivo* experimental scheme. 8µg NU7441 or vehicle (4% DMSO in PBS) were administered intra peritoneally (i.p.) to WT, *Sting-/-* and *Ifnar-/-* mice 1h before challenge with diABZI (1µg, i.p). Parameters were analyzed 6 hours after the last administration.

(J) Gene expression analyses were conducted in peritoneum of mice treated as in I (n=3-8 mice per group). Graphs present the mean (±SEM). Statistical significance was calculated by 2-tailed Student T-test.

(K) Gene expression analyses were conducted in peritoneal macrophages of mice treated as in I (n=4-8 mice per group). Graphs present the mean (±SEM). Statistical significance was calculated by 2-tailed Student T-test.

(L) Gene expression analyses were conducted on the spleen of mice treated as in I (n=3-8 mice per group). Graphs present the mean (±SEM). Statistical significance was calculated by 2-tailed Student T-test.

(M) Concentration of Cxcl10 in the peritoneal fluid of mice treated as in I was determined by ELISA (n=3-8 mice per group). Graph presents the mean (±SEM). Statistical significance was calculated by 2-tailed Student T-test.

(N) The concentration of Cxcl10 in the spleen of mice treated as in I (n=3-8 mice per group) was determined by ELISA. Graph presents the mean (±SEM). Statistical significance was calculated by Student T-test.

****: $p<0.0001$; ***: $p<0.001$; **: $p<0.01$; *: $p<0.05$; ns: not significant.

Also see Figure S4.

Figure 5. DNA-PKcs regulates antiviral responses towards DNA and RNA virus infection.

(A) Experimental scheme: T98G cells were treated with 10µM diABZI, 1µM E7766 or 10µg/ml fluorinated 3’3’-cGAMP in combination of not with 2µM of NU7441 Cells were subsequently infected or not with HSV-1 for 48 hours Cells were subsequently infected or not with HSV-1 for 48 hours, prior to DAPI nuclear staining and image acquisition.

(B) Image acquisition of T98G cells treated as in A, GFP (yellow) indicates HSV-1 viral load. Images are representative of 3 independent experiments.

(C) Quantification of HSV-1 infected signal in experiments conducted as in A. Graph presents the mean (±SEM) **of 3 independent experiments**. Statistical significance was calculated by Student T-test.

(D) As in C, except that treated cells were infected with MPXV clade 2b strain S2626 for 48 hours. Graph presents the mean (±SEM) **of 3 independent experiments**. Statistical significance was calculated by Student T-test.

(E) As in C, except that treated cells were infected with VSV for 16 hours. Graph presents the mean (±SEM) **of 3 independent experiments**. Statistical significance was calculated by Student T-test.

(F) Human primary macrophages were treated with 10µg/ml fluorinated 3'3'-cGAMP in combination of not with 2µM of NU7441, prior to infection with VSV for 48 hours, prior to DAPI nuclear staining and image acquisition. Images are representative of 3 independent experiments.

(G) Graph presents the mean (±SEM) VSV infected cells when treated as in F. Statistical significance was calculated by Student T-test.

(H) Experimental scheme. T98G cells were either treated with 2 µM NU7441 for 1 hour prior to infection and gene expression analysis at 6 and 16 hours post-infection (*pre-treatment*) or infected for 6 hours prior to treatment with NU7441 and gene expression analysis at 16 hours post-infection (*post-treatment)*.

(I) Gene expression analysis in cells 'pre-treated' and 'post-treated' as described in H. Graph presents the mean (±SEM) of 3 independent experiments. Statistical significance was calculated by Student T-test.

****: $p<0.0001$; ***: $p<0.001$; **: $p<0.01$; *: $p<0.05$; ns: not significant.

See also Figure S5

Data availability: Correspondence and requests for material should be addressed to Nadine Laguette or Dimitrios Vlachakis. Raw data for Immunoblots are provided with the manuscript.

Author contributions: Conceptualization: NL, DV; Methodology: IKV, CT , YMN, NL, DV, SG, AA; Investigation: IKV, CT, MSchussler, PLH, JB, JJ, YMN, JMK, TC, JP, JR, FP, FGB, RL, KT, MC, IEM, AA, RJE, MSerbier, SG, FDG; Visualization: IKV, CT, DV, NL; Funding acquisition: NL, KM, NB; Project administration: NL; Supervision: NL, DV, IKV, GPC, NB, KM, FPB, OS; Writing – original draft: NL; Writing – review & editing: NL, DV, IKV, CT, YMN, MSchussler, JJ, JMK, KM, NB, DV, FPB, OS.

Acknowledgments: We thank all members of the Molecular Basis of Inflammation laboratory for reading and editing the manuscript. We thank Caroline Bertin, Johanna Marines, Amel Bouzid, Amandine Kremer, Mathilde Saccas, Robin Charpentier and Tommy Chastel for technical assistance. We thank Soren Paludan for control, STING- and cGAS-deficient THP-1 cell lines and HSV-1-GFP. We thank Dr. Jin Lei for the gift of Sting-deficient mice, we thank Dr. Miereia Pellegrin for the gift of Ifnar-deficient mice. We thank Dr. Christelle Langevin for the gift of the VSV-GFP molecular clone. We thank the ZEFI and the PCEA animal facilities for animal housing. We thank the CEMIPAI BSL3 level laboratory for housing virology experiments. We acknowledge the MRI imaging facility, member of the national infrastructure France-BioImaging infrastructure supported by the French National Research Agency (ANR-10-INBS-04, “Investments for the future”). We thank the MAMMA metabolomics platform for support.

This work was co-funded by the European Union (ERC, SENTINEL 101087092 to NL; DELV to KM). Views and opinions expressed are however those of the author(s) only and do not necessarily reflect those of the European Union or the European Research Council. Neither the European Union nor the granting authority can be held responsible for them. This work was also co-funded by : the ANR [AlphA(NL), dezincRNA to (KM)]; l’Institut National du Cancer INCa_1884 (NB) and Inca_19379 (NL)]; LA Ligue pour la recherche contre le cancer [AAPARN 2021.LCC/JuF (NL), équipe labellisée (NB)], the Agence Nationale de Recherche sur le SIDA et les Hépatites virales (ANRS) [ECTZ117448 (NL) and fellowships to CT and JMK], the I-SITE Excellence Program of the University of Montpellier, under the Investissements France 2030 [RETTiNA (NL), ChoiCe (NL)], the Fondation ARC [ARCPJA2021060003720 COPALYS (NL), ARCPJA2021060003886 (NB)], La Région Languedoc Roussillon [Prématuration 2021 MODULON 21015964 (NL)], Fondation de France [fellowship (JJ)], Fondation pour la Recherche Médicale [SPF202409019744 (YMN)], and the Centre National de La Recherche Scientifique [Prématuration CNRS (NL)]. The O.S. lab is funded by Institut Pasteur, Fondation

pour la Recherche Médicale (FRM), ANRS, the Vaccine Research Institute (VRI) (ANR-10-LABX-77), Labex IBEID (ANR-10-LABX-62-IBEID), the HERA projects DURABLE (grant 101102733) and LEAPS. JP is supported by DURABLE. This work was also supported by the ANRS (ECTZ192763) and the ANR (ANR-23-CE15-0028 METABODEN) to FPB.

Competing interests: Authors declare that they have no competing interests.

Supplementary Figure Legends

Figure S1. 2'3'-cGAMP interacts with the catalytic pocket of DNA-PKcs.

(A) Experimental scheme for **B**. Whole cell extracts (WCE) from T98G cells were used as input for IPs using mock IgG and DNA-PKcs-specific antibodies prior to incubation with 2'3'cGAMP and detection of bound 2'3'cGAMP.

(B) WB analysis of DNA-PKcs IP performed as in **A** was conducted using the indicated antibodies. **Representative WB of 3 independent experiments**.

(C) Graph represents mean (±SEM; **n=3 independent experiment**) 2'3'-cGAMP levels as measured in Mock and DNA-PK-specific IP performed as in **A**. Statistical significance was calculated by 2-tailed Student T-test.

(D) Silver-staining was conducted on recombinant DNA-PKcs used in Figure 2 for immunoprecipitation experiments **Representative gel of 3 independent experiments**.

(E) WB analysis of thermal shift assay (TSA), conducted on WCE from THP-1 cells incubated with or without 2'3'-cGAMP or in presence or not of NU7441. Immunoblot was performed using DNA-PKcs, STING and HSP90 specific antibodies. **Representative WB of 3 independent experiments**.

(F) Heatmap representation of the relative band intensities quantified from 3 independent experiments performed as in **E.**

(G) Molecular modelling and docking study of 2'3'-cGAMP into DNA-PKcs. Left: Human DNA-PKcs in ribbon representation with 2'3'-cGAMP docked in its catalytic site.

(H) The docking conformation of 2'3'-cGAMP (in red spacefill representation) into the catalytic site of DNA-PKcs in the proximity of the catalytic residues (in ball and stick representation).

(I) The docked conformation adopted by 2'3'-cGAMP onto the catalytic site of DNA-PKcs upon the Molecular Dynamics simulations.

(J) The 2D molecular interactions diagram of 2'3'cGAMP with the catalytic residues of DNA-PKcs.

(K) Molecular modelling of ATM and ATR. DNA-PKcs superposed to the models of ATM and ATR (in red, blue and yellow ribbon representations respectively).

(L) Close-up of the superposed active sites of ATM, ATR and DNA-PKcs. Each of the 3 kinases has significant conformational differences and docking of 2'3'-cGAMP to all of them failed to return a thermodynamically viable pose (complex conformation).

(M) Experimental scheme for N. Recombinant DNA-PKcs was immunoprecipitated using a DNA-PKcs-specific antibody, prior to incubation or not with increasing doses of NU7441 inhibitor (0, 0.2, 2, 20 µM) followed by 2'3'-cGAMP incubation, release of bound 2'3'-cGAMP, and detection by ELISA

(N) Graph represents mean (±SEM) 2'3'-cGAMP levels as measured in DNA-PK-specific IP performed as in **M**. **n=3 independent experiments** Statistical significance was calculated by 2-tailed Student T-test.

****: p<0.0001; ***: p<0.001; **: p<0.01; *: p<0.05; ns: not significant.

Related to Figure 1.

Figure S2. DNA-PKcs dampens 2'3'cGAMP-mediated STING signaling

(A) Graph represents mean (±SEM, n=3 independent experiment) CXCL10 and CCL5 levels as measured in supernatant of T98G cells treated or not with 2µM NU7441 for 1 hour prior to transfection or not of 10µg/ml 2'3'-cGAMP for 6 hours. Statistical significance was calculated by 2-tailed Student T-test.

(B) T98G cells were pretreated with the NU7441 (2µM), NU7026 (10µM) and AZD7648 (5µM) DNA-PKcs inhibitors for 1 hour prior to transfection of 2'3'-cGAMP (10µg/mL) for 6 hours and gene expression analysis. Graphs present the mean (±SEM, n**=3 independent experiments**). Statistical significance was calculated by two-tailed Student T-test.

(C) T98G cells were pretreated with the NU7441 (2µM) for 1 hour prior to transfection with dsDNA (2µg) for 6 hours and gene expression analysis. Graphs present the mean (±SEM, **n=3 independent experiments**). Statistical significance was calculated by two-tailed Student T-test.

(D) T98G cells were transfected for DNA-PKcs- or KU70-targeting siRNAs or a control non targeting siRNA for 48 hours prior analysis of knockdown efficiency by WB using the indicated antibodies. **Representaitve WB, n=3 independent experiments**.

(E) T98G cells were engineered to express control non-targeting or PRKDC-targeting gRNA. **Representative WB, n=3 independent experiments**.

(F) THP-1 CTRL, THP1 $^{cGAS-/-}$ and THP1 $^{STING-/-}$ were pretreated or not with the NU7441 (2µM) inhibitor for 1h prior to transfection in presence or absence of 2'3'-cGAMP (10µg/mL) for 6h. WB analysis was performed using the indicated antibodies. Representative WB, of 3-5 **independent experiments.**

(G) Densitometric quantification of band intensities of the p-IRF3/IRF3 ratio from the WB in **F**. Results shown as % of induction of 2'3'cGAMP response (n=3-5 **independent experiments**).

(H) Densitometric quantification of band intensities of the p-STING/STING ratio from the WB in **F**. Results shown as % of induction of 2'3'cGAMP response (n=3-5 **independent experiments**).

(I) Graph represents mean (±SEM, n=3 independent experiment) IFNβ levels as measured in supernatant of THP1 CTRL, THP1 $^{cGAS-/-}$ and THP1 $^{STING-/-}$ pretreated or not with the NU7441 (2µM) inhibitor for 1h prior to transfection in presence or absence of 2'3'-cGAMP (10µg/mL) for 6h. Statistical significance was calculated by 2-tailed Student T-test.

(J) T98G cells were engineered to express control non-targeting or PRKDC-targeting gRNA. **Representative WB of 3 independent experiments**.

(K) T98G cells engineered to express control non-targeting or STING-targeting gRNAs were treated or not with 2µM of NU7441 prior to Mock transfection or transfection of 10µg/ml 2'3'-cGAMP and gene expression analysis. Graphs present the mean (±SEM, n=5 **independent experiments**). Statistical significance was calculated by two-tailed Student T-test.

(L) As in **K** except that WB analysis was performed using the indicated antibodies. **Representative WB of 3 independent experiments**.

(M) As in **L**, except that T98G cells expressing an IFNAR-targeting gRNA were used. **Representative WB of 3 independent experiments**.

(N) THP-1 cells were pretreated or not with the NU7441(2µM) inhibitor for 1h prior to transfection with dsDNA (2µg) for up to 24h. Gene expression analysis was conducted at 3, 6, 16 and 24 hours. Graphs present the mean (±SEM, **n=3 indepent experiments**). Statistical significance was calculated by two-tailed Student T-test.

(O) Cell culture supernatants were collected at 24 hours in experiment performed as in N, and cytokine/chemokine levels were analysed using a proteome profiler array. Heatmap representation of relative spot intensities is shown (**mean of 3 independent experipments**).

(P) STING-deficient THP-1 cells engineered to express human STING haplotypes (STING-H232, STING-AQ, STING-HAQ) were pretreated or not with the NU7441 (2µM) for 1h prior to transfection of 2'3'-cGAMP (10µg/mL) for 6h and gene expression analysis. Graphs present the mean (±SEM, n=3 independent experiments). Statistical significance was calculated by two-tailed Student T-test.

(Q) As in **P** except that IFNβ and CXCL10 levels were quantified by ELISA in supernatants. Graphs present the mean (±SEM, n=3 independent experiments). Statistical significance was calculated by two-tailed Student T-test.

***: $p<0.001$; **: $p<0.01$; *: $p<0.05$; ns: not significant.

Related to Figure 2.

Figure S3. DNA-PKcs selectively counteracts CDNs.

(A) ATP hydrolysis by DNA-PKcs was measured in vitro in presence of increasing doses (0.8 µM to 2500 µM) of c-di-GMP. Graph presents the mean (±SEM) performed in biological triplicates. Statistical significance was calculated by **one-way ANOVA**. ns: not significant.

(B) T98G cells were treated or not with 2 µM NU7441 in combination or not with 10µg/ml fluorinated 3'3'-cGAMP for 6 hours prior to WB analysis using the indicated antibodies. Representative WB of 3 independent experiments.

(C) As in B, except that gene expression analyses were conducted. Graphs present the mean (±SEM) performed in biological triplicates. Statistical significance was calculated by two-tailed Student T-test. ***: $p<0.001$; **: $p<0.01$; *: $p<0.05$.

(D) Experimental scheme for Human primary monocyte isolation and treatment (Figure 3E). Human primary monocytes were isolated from buffy coats prior to treatment or not with 2µM NU7441 for 1 hour followed by administration of 10µg/ml fluorinated 3'3'-cGAMP for 6 hours and gene expression analysis.

(E) Flow cytometry analysis of macrophages prepared as in **Figure 3G**.

(F) Gene expression analyses was performed on human primary cells treated as described in **Figure 3G**. Graphs present the mean (±SEM) expression of *IFIT1* in 3 independent experiments. Statistical significance was calculated by 2-tailed Student T-test.

(G) T98G cells were treated or not with 2µM of NU7441 prior to addition or not of 1 µM of E7766 STING agonist for 3 hours and analysis of gene expression. WB analysis were conducted using indicated antibodies and are representative of 3 independent experiments.

(H) T98G cells were treated or not with 2µM of NU7441 prior to addition or not of 50µM of ADU-S100 STING agonist for 3 hours and analysis of gene expression. WB analysis were conducted using indicated antibodies and are representative of 3 independent experiments.

(I) T98G cells were treated or not with 2µM of NU7441 prior to addition or not of 10µM of diABZI for 3 hours and analysis of gene expression. WB analysis were conducted using indicated antibodies and are representative of 3 independent experiments.

(J) Control and DNA-PKcs knockout THP-1 cells were treated with 1µM E7766 for 6 hours prior to gene expression analysis. Graphs present mean (±SEM), **n=3 idependent experiments**. Statistical significance was calculated by 2-tailed Student T-test.

(K) Control and DNA-PKcs knockout THP-1 cells were treated with 10µM diABZI for 6 hours prior to gene expression analysis. Graphs present mean (±SEM), **n=3 independent experiments**. Statistical significance was calculated by 2-tailed Student T-test.

***: p<0.001; **: p<0.01; *: p<0.05.

Related to Figure 3.

Figure S4. DNA-PKcs inhibits STING agonists-induced inflammatory responses in murine models.

RAW264.7 cells were treated or not with NU7441 1h before stimulation with 10µM diABZI or 1µM E7766) for 6h prior to gene expression analyses. Graphs present the mean (±SEM) of 3 independent experiments. Statistical significance was calculated by One-way Anova with multiple comparison.

***: p<0.001; ns: non-significant.

Related to Figure 4.

Figure S5. DNA-PKcs decreases the ability of STING agonists to trigger an antiviral response.

(A) T98G cells were treated with the 10µM diABZI, 1µM E7766 or 10 mg/mL Fluorinated 3'3'-cGAMP in combination or not with 2µM of NU7441. Cells were subsequently infected or not with VSV-GFP for 16 hours, prior to DAPI nuclear staining and image acquisition. Images are representative of 3 independent experiments.

(B) As in A, except that cells were infected with the MPXV clade 2b strain S2626 for 48 hours. Images are representative of 3 independent experiments.

(C) T98G cells engineered to express control non-targeting or DNA-PKcs targeting gRNA were treated with 10 µg/mL Fluorinated 3'3'-cGAMP in combination or not with 2 µM of NU7441. Cells were subsequently infected or not with VSV-GFP at MOI 0.3 for 16 hours, prior to DAPI nuclear staining and image acquisition. Graph shows the mean (± SEM, **n=3 independent experiments**) percentage of infected (GFP^+) cells as measued by florescent microscopy. Statistical significance was assessed using 2-tailed Student T-test.

(D) Gating strategy for macrophages used in Figure 5E.

(E) Histograms show the percentage of infected (GFP^+) cells as measured by flow cytemotry, following treatment with STING agonists, in the presence or absence of NU7441, at two different MOIs.

(F) DNA-PKcs inhibition (NU7441) enhances anti-viral state against VSV in primary macrophages. Primary macrophages from healthy donors 1, 2 and 3 where pretreated with NU7441 prior STING agonist treatment. Cells treated with a STING agonist, were set as 100% infection and the effect of adding a NU7441 was assessed relative to this condition.

**: $p<0.01$; *: $p<0.05$. Data are from at least three independent experiments.

Related to Figure 5.

Methods

Cells and Cell Culture:

T98G cells were a gift from Caroline Goujon (IRIM, Montpellier, France). Control THP-1, cGAS-deficient THP-1 (THP-1$^{cGas-/-}$) and STING-deficient THP-1 (THP-1$^{Sting-/-}$) were a gift of S. R. Paludan (Aarhus university, Aarhus, Danemark). Vero (African green monkey), HEK293T (*Homo sapiens*) and THP-1 (*Homo sapiens*) cells were obtained from the American Type Culture Collection (ATCC).

T98G$^{STING-/-}$, T98G$^{IRF3-/-}$ and their control counterparts were previously generated using the CRISPR-Cas9 technology (Taffoni et al., 2023). Parental and genetically engineered T98G, HEK293T, and Vero cells were maintained in Dulbecco's Modified Eagle Medium (DMEM) supplemented with 10 % Fetal Bovine Serum (FBS, Eurobio), 1% L-glutamine (Lonza), 1% Penicillin/Streptomycin (Lonza). THP-1 cells (Cat#TIB-202, ATCC) were cultured in Roswell Park Memorial Institute (RPMI, Lonza) supplemented with 20% FBS, 1% penicillin/streptomycin and 1% L-glutamine. All cell lines were maintained at 37 °C, under 5% CO_2.

Primary monocyte isolation from human blood and MDM differentiation for gene expression analyses

Buffy coats were obtained from the Etablissement Français du Sang (EFS, Nantes, France). Human primary monocytes were isolated using the StraightFrom Buffy Coat CD14 Microbead Kit (Miltenyi) and differentiated into macrophages for 5 days using 10µg/mL GM-CSF.

Primary monocyte isolation from human blood and MDM differentiation for virus infection

Buffy coats from healthy donors were obtained from the Etablissement Français du Sang (EFS, Montpellier, France). CD14^{+} monocyte isolations from 3 healthy donors were performed using the EasySep™ Human CD14 Positive Selection Kit II (Stemcell Technologies, #17858) and differentiated straight towards monocyte-derived macrophages (MDM) upon 5-7 days incubation with 500 U/ml M-CSF in IMDM medium supplemented with 10% FBS, 100 U/ml penicillin, 100 µg/ml streptomycin, 1mM HEPES (Sigma, H3537-100ML), 1 mM Sodium pyruvate (Sigma, S8636-100ML) and 1X MEM Non-Essential Amino Acids (Sigma, M7145-100ML). Expression of the following macrophages markers were routinely analysed by flow cytometry for each donor: CD14, CD68, and HLA-DR.

THP-1 cells expressing human STING haplotypes

THP-1 cells stably expressing human STING haplotypes were generated using THP1-Dual™ KO-STING as detailed in (Guha et al., 2025). In brief, cells were transduced with retroviral vectors expressing N-terminal HA-tagged HsSTING haplotypes/mutants (HsSTING-R232H, HsSTING-AQ, HsSTING-HAQ) and selected with 2 µg/ml puromycin.

Mice and mouse housing conditions

Wild-type (WT) mice and mice deficient for STING (*Sting-/-*) and IFNAR (*Ifnar-/-*) were bred and housed under pathogen-free conditions at CNRS animal facility (ZEFI UMR5535, Montpellier, France). Mouse strains are C57/BL6J and backcrosses to reference strains are performed every 5 generations. They were maintained in a 12-h light-dark cycle with food and water ad libitum, following European and local legislation. Age-matched, 8- to 14- week-old mice were used for experiments. All animal experiments complied with the French Government animal experiment regulations and ARRIVE guidelines. The protocols were submitted to the "Ethics Committee for Animal Experimentation of CNRS Campus Montpellier under numbers (G3417216) and approved by the French Minister under APAFIS #41092.

Drugs

NU7441 Biotechne/Tocris, #3712, **CID:** 11327430
DMSO Sigma, D2650, **CID:** 679
2'3'-cGAMP InvivoGen, tlrl-nacga23-02, **CID:** 137120248
3'3'-cGAMP InvivoGen, tlrl-nacga, **CAS number:** 849214-04-6
c-di-AMP InvivoGen, tlrl-nacda, **CAS number:** 2734909-87-4 / 54447-84-6 (free acid)
c-di-GMP InvivoGen, tlrl-nacdg, **CAS number:** 2222132-40-1 / 61093-23-0 (free acid).
diABZI InvivoGen, tlrl-diabzi-2, **CID:** 137701219, **CAS number:** 2138299-34-8
E7766 MedChemExpress, HY-111999A,
ADU-S100 ammonium salt MedChemExpress, HY-12885B
Fluorinated 3'3'-cGAMP Invivogen, tlrl-nacgaf-05, **CAS number**: not available

Generation of T98G knock-out cell lines

To generate the T98G$^{IFNAR-/-}$ knock-out and control cell lines, lentiviral particles were produced by co-transfection of 2×10^6 293T cells with 5 µg of LentiCRISPRv2GFP plasmid (Addgene # 82416) expressing the gRNA targeting the gene of interest or non-targeting control (CTRL) gRNA, 5 µg of psPAX2 and 1 µg of pMD2.G, using the standard calcium phosphate transfection protocol.

T98G cells were transduced with lentiviral particles and 72 hours post-transduction GFP-positive cells were sorted and pooled in a 6-well plate using a BD FACS melody. Cells were next amplified and IFNAR levels controlled by WB.

HEK293T$^{DNA\text{-}PKcs\text{-}/\text{-}}$ clones and HEK293T^{CTRL} cells were generated by JetPrime (Polyplus) mediated transfection of LentiCRISPRv2GFP plasmid expressing the gRNA targeting the gene of interest or non-targeting control (CTRL) gRNA. Two days later GFP^{+} single-cell clones were selected on a BD FACSAria. Absence of DNA-PK expression was verified by WB.

<u>Primers for gRNA expressing constructs:</u>

CTRL:
CACCGAGCACGTAATGTCCGTGGAT, AAACATCCACGGACATTACGTGCTC
IFNAR:
CACCGAGCTGACACTCACCTTCCCC, AAACGGGGAAGGTGAGTGTCAGCTC
PRKDC:
CACCGGCAGGAGACCTTGTCCGCTG, AAACCAGCGGACAAGGTCTCCTGCC

<u>Generation of THP-1 Knockout Cells by CRISPR/Cas9</u>

DNA-PK–knockout THP-1 cells were generated using the CRISPR/Cas9 ribonucleoprotein (crRNP) gene-editing system according to the manufacturer's instructions (Synthego) and has described in (Rabinowitz et al., 2025). Briefly, purified recombinant Cas9 protein was complexed with target-specific single-guide RNA (sgRNA) to form Cas9–sgRNA ribonucleoprotein (RNP) complexes by incubation for 10 minutes at room temperature immediately prior to delivery. Cas9 RNPs were introduced into THP-1 cells by nucleofection using the Lonza 4D-Nucleofector System, optimized for THP-1 cells with the SG Cell Line 4D-Nucleofector® X Kit S (Lonza; Catalog #V4XC-3032). Transient delivery of Cas9 RNPs enables efficient genome editing while minimizing prolonged Cas9 expression and reducing off-target effects. To generate stable knockout cell lines, edited cells were single-cell cloned by limiting dilution. Individual clones were expanded and validated at both the genomic and protein levels to confirm biallelic gene disruption.

<u>Cloning of DNA-PK expression vector:</u>

pcDNA3.1-nFlag-DNA-PK was cloned from synthesized gene fragments (eBlocks, IDT) based on consensus sequence ENST00000314191.7 modified for codon optimization. The gRNA binding site targeted for knock-out was modified to prevent targeting by CRISPR/Cas9

constructs. N-terminal 3XFlag sequence including $(GGGGS)_3$ linker was added to the synthesized template. pcDNA3.1 backbone was digested using BamHI and EcoRI, dephosphorylated using Quick CIP (NEB) and purified on agarose gel. eBlocks were amplified with KAPA HIFI HotStart Ready Mix (Roche) and purified on agarose gel. Gibson cloning was performed in two steps, with amplified and purified intermediate constructs, using NEBuilder HiFi DNA Assembly Master Mix and NEB Stable Competent *E. coli* grown at 30°C. Resulting plasmid preparations were verified by whole plasmid sequencing.

Gene silencing

Silencing of DNA-PKcs was achieved in T98G cells using siRNAs and INTERFERin (Polyplus) following the manufacturer's instructions. siRNAs (Dharmacon™; Horizon Discovery) were used:

siCTRL: CGUACGCGGAAUACUUCGAUU
siDNA-PKcs: GAUCGCACCUUACUCUGUUUU
siKU70: ACAAGCAGUGGACCUGACUU

Cell treatment and transfection

Cells were plated in 6-well plate, or 100 mm dishes. Eighteen hours later, cells were pretreated with 2 µM NU7441 (#3712, Biotechne/Tocris) for 1 hour in DMEM or RPMI, prior to transfection with 2′3′-cGAMP (10 µg/ml, InvivoGen) using Lipofectamine 2000 (Thermo Fischer Scientific), following the manufacturer's instructions. One, three or six hours after transfection, cells were harvested and stored at −80°C prior to 2’3’-cGAMP, protein or RNA extraction.

For other drug treatment, following 1 hour preincubation with Nu7441, cells were treated with 2’3’-GAM(PS)2 (Rp/Sp) (InvivoGen), or fluorinated 3’3’-cGAMP (InvivoGen) at 10 µg/ml, with diABZI compound 3 (InvivoGen) at 10 µM, with E7766 (MedChemExpress) at 1 µM, or ADU-S100 (MedChemExpress) at 50µM. Six hours later, cells were harvested and stored at −80°C prior to protein or RNA extraction.

Mouse treatment

Mice were pretreated intraperitoneally (i.p.) with either NU4474 (8 µg in 200 µL) or DMSO (4% in 200 µL) one hour before being challenge with the diABZI (1 µg in 200 µL C or PBS. After 6 hours, the mice were euthanized.

Peritoneal lavage (PL) was performed 6h after the last challenge by rinsing the peritoneal cavity with 5 mL of cold PBS via a cannula inserted in the peritoneum.

The acellular fraction of the lavage (supernatant) was collected after centrifugation and was used to asses Cxcl10 by ELISA. The cellular fraction containing peritoneal macrophage was used for the quantification of mRNA expression by RT-qPCR. The peritoneum and spleen were collected for gene expression analysis and Cxcl10 production measurement.

RNA extraction and gene expression analyses

Total RNA was isolated with TRIzol (Invitrogen). RNA concentration was measured with a Nanodrop spectrophotometer (ND-1000, Nanodrop Technologies), prior to treatment with TURBO DNase (Ambion) and cDNA synthesis from 1-2 µg RNA using SuperScript IV (Invitrogen) using Oligo(dT) and quantification with a LightCycler 480 cycler (Roche) using SYBR Green Master Mix (Takara) and appropriate primers. Relative quantities of the transcript were calculated using the ΔΔCt method, using the Glyceraldehyde3-phosphate dehydrogenase (*GAPDH*) for normalization, except for THP1 analyses were a normalization with Hypoxanthine Phosphoribosyltransferase 1 (*HPRT1*) and Actin Beta (*ACTB*) was performed. For normalization in mouse cell lines, *Glyceraldehyde3-phosphate dehydrogenase* (*Gapdh*) or *Heat Shock Protein 90* (*Hsp90*) were used. The RT-qPCR primers used are listed below:

GAPDH: For: CTGGCGTCTTCACCACCATGG, Rev: CATCACGCCACAGTTTCCCGG
ACTB: For: GGACTTCGAGCAAGAGATGG, Rev: AGCACTGTGTTGGCGTACAG
HPRT1: For: TGACACTGGCAAAACAATGCA, Rev: GGTCCTTTTCACCAGCAAGCT
IFNB1: For: GAATGGGAGGCTTGAATACTGCCT, Rev: TAGCAAAGATGTTCTGGA GCATCTC
ISG15: For: GATCACCCAGAAGATCGGCG, Rev: GTTCGTCGCATTTGTCCACC
CXCL10: For: GAAAGCAGTTAGCAAGGAAAGGTG, Rev: ATGTAGGGAAGTGATG GGAGAGG
IFIT1: For: GCCTTGCTGAAGTGTGGAGGAA, Rev: ATCCAGGCGATAGGCAGAGATC
IFIT2: For: GGAGCAGATTCTGAGGCTTTGC, Rev: GGATGAGGCTTCCAGACTCCAA
CCL5: For: CCTGCTGCTTTGCCTACATTGC, Rev: ACACACTTGGCGGTTCTTTCGG

Gapdh: For: TTCACCACCATGGAGAAGGC, Rev:GGCATCGACTGTGGTCATGA
Hsp90: For: GTCCGCCGTGTGTTCATCAT, Rev: GCACTTCTTGACGATGTTCTTGC
Ifnb:For:CTGCGTTCCTGCTGTGCTTCTCCA, Rev:TTCTCCGTCATCTCCATAGGGATC
Cxcl10: For:ATGACGGGCCAGTGAGAATG, Rev: TCAACACGTGGGCAGGATAG
Ccl5: For:CAGCAAGTGCTCCAATCTTGC, Rev:CCACTTCTTCTCTGGGTTGGC
Ifit1: For:TTTCCGTAGGAAACATCGCGT, Rev:TGTTGCTTGTAGCAGAGCCC
Isg15: For:GTGCTCCAGGACGGTCTTAC, Rev:CTCGCTGCAGTTCTGTACCA

Il6: For:GACTTCCATCCAGTTGCCTTCT, Rev:TTCTCTCCGGACTTGTGAAGT
Tnfα: For:CTGTAGCCCACGTCGTAGC, Rev:TTGAGATCCATGCCGTTG

Measurement of cytokine levels

IFNβ, CCL5 and CXCL10 concentrations in the peritoneal lavage or spleen were measured by ELISA (R&D System, Minneapolis) according to manufacturers' instructions. Data were acquired on the FLUOstar Omega equipment (BMG-LABTECH, Germany).

Whole-cell lysate preparation and Western Blot

Cells were lysed in 5 packed cell volumes of TENTG-150 (20 mM Tris–HCl [pH 7.4], 0.5 mM EDTA, 150 mM NaCl, 10 mM KCl, 0.5% Triton X-100, 1.5 mM MgCl2, and 10% glycerol, supplemented with 10 mM β-mercaptoethanol, 0.5 mM PMSF and phosphatase inhibitor (Sigma)) for 30 min at 4°C. Lysates were centrifuged 30 min at 14,000 g, and supernatants were collected for WB. Protein quantification was performed using Bradford assay (Bio-Rad).

Protein samples were prepared in Laemmli buffer and heated at 95°C for 5 min prior to resolution by sodium dodecyl sulfate–polyacrylamide gel electrophoresis (SDS-PAGE) using 4–15% Mini-PROTEAN® TGX™ Precast Protein Gels (Bio-Rad). Proteins were transferred onto nitrocellulose membranes (Biorad Trans blot turbo). Proteins were visualized on membranes using Ponceau S solution (Sigma-Aldrich) prior to 30 min blocking with (PBS) containing 0.1% Tween (PBS-T) supplemented with 5% milk. Membranes were subsequently incubated with primary antibodies in 5% milk/PBS-T (1:1,000 dilution, except when indicated) for 2 hours at RT. Primary antibodies used include: anti-DNA-PKcs (A300-517, Bethyl, 1:500), anti-cGAS (15102) Cell Signaling Technology), anti-pSTING Ser366 (19781, Cell Signaling Technology), anti-STING (13647, Cell Signaling Technology), anti-pIRF3 Ser386 (ab76493, Abcam), anti-IRF3 (11904, Cell Signaling Technology), anti-HSP90 (4877, Cell Signaling Technology), anti-GAPDH (60004-1-Ig, Proteintech Europe, 1:5,000), αTUBULIN (66031-1-Ig, Proteintech Europe, 1:10,000). Membranes were incubated with Horseradish peroxidase (HRP)-coupled secondary antibodies (Cell Signaling Technology) at 1:2,000 dilution, for 1 hour at RT. Immunoreactivity was detected by Chemiluminescence (SuperSignal West Pico or Femto, Thermo Fisher Scientific). Images were acquired on a ChemiDoc (Bio-Rad) or Amersham Imager 680 (GE Healthcare).

Endogenous DNA-PKcs and FLAG-DNA-PKcs immunoprecipitation and assessment of interaction with 2'3'-cGAMP interaction

For immunoprecipitation of endogenous DNA-PKcs, T98G cells were lysed in 5 packed cell volume of the lysis buffer 20 mM Tris–HCl [pH 7.4], 150 mM NaCl, 10 mM KCl, 0.5% Triton X-100, 1.5 mM MgCl2, and 10% glycerol, supplemented with 10 mM β-mercaptoethanol, 0.5 mM PMSF, for 30 min at 4°C on a wheel. Lysates were centrifuged 30 min at 14,000 g, and supernatants were collected for immunoprecipitation. Endogenous immunoprecipitation was performed using DNA-PKcs-targeting antibody (A300-517A, Bethyl), or Rabbit IgG (Santa Cruz) as a negative control. After an overnight incubation at 4°C on a wheel, immunoprecipitation was performed using Protein G Sepharose Fast Flow beads (Sigma). After 3 washes in lyses buffer, part of the bound material was either eluted in Laemmli buffer for WB analyses, or used to assess DNA-PKcs:2'3'-cGAMP interaction.

FLAG-DNA-PKcs immunoprecipitation was performed by expressing FLAG-DNA-PKcs in 293T$^{DNA\text{-}PKcs\text{-}/\text{-}}$ for 48 hours prior to whole cell extract preparation as above and immunoprecipitation using anti-FLAG dynabeads. Immunoprecipitates were analyzed by WB or used to assess DNA-PKcs:2'3'-cGAMP interaction

To assess DNA-PKcs:2'3'-cGAMP interaction, bound material was incubated with an excess of 2'3'-cGAMP diluted in lyses buffer, for 30 min on ice. After 3 washes with lyses buffer, bound material was subjected to proteinase K treatment (15 min at room temperature) to denature DNA-PKcs and allow the release of potential bound 2'3'-cGAMP. Proteinase K were inactivated, incubating samples 10 min at 95°C, prior to measurement of 2'3'-cGAMP level by enzyme-linked immunosorbent assay (ELISA).

<u>Immunoprecipitation of Recombinant DNA-PKcs and assessment of interaction with CDN</u>

For the immunoprecipitation of recombinant DNA-PKcs, 2 µg of anti-DNA-PKcs antibody or the corresponding IgG control was incubated with 70 ng of recombinant DNA-PKcs protein (Promega) in 500 µL of lysis buffer (20 mM Tris–HCl [pH 7.4], 150 mM NaCl, 10 mM KCl, 0.5% Triton X-100, 1.5 mM MgCl2, and 10% glycerol, supplemented with 10 mM β-mercaptoethanol, 0.5 mM PMSF). The mixture was incubated overnight at 4°C on a rotating wheel. The next day, the samples were centrifuged at 12,000 rpm for 10 min, and the supernatant was collected. Thirty µL of Sepharose beads (5 µL per immunoprecipitation point, for a total of 6 points) were added to the supernatant and incubated at 4°C for 45 min on a rotating wheel. Following incubation, the beads were centrifuged at 2,500 rpm and washed three times with the lysis buffer (without β-mercaptoethanol and PMSF). After washing, the immunoprecipitated complexes were incubated with the tested cyclic dinucleotides (CDNs), including 2'3'-cGAMP, 3'3'-cGAMP, and c-di-AMP, with or without NU7441. The incubation was performed with a CDN or nu7441 concentration 10 times higher than that of DNA-PKcs for 30 min on ice. After

the incubation, the beads were washed, and the samples were digested with proteinase K before measuring the amount of CDNs bound to DNA-PKcs by ELISA. 2’3’-cGAMP, 3’3’-cGAMP and c-di-AMP ELISA were performed according to the manufacturer's protocol using the Cayman Chemical 2′3′-cGAMP ELISA Kit (CAY501700), 3′3′-cGAMP ELISA Kit (CAY502130), c-di-AMP ELISA Kit (CAY501960), respectively.

ATP hydrolysis assay

The ability of DNA-PK to hydrolyze ATP was measured by using the DNA-PK Kinase Enzyme System coupled to the ADP-Glo Assay (Promega), following manufacturer’s instructions. Briefly, 30 unit of human recombinant DNA-PK were incubated for 60 min at room temperature with 1 µM ATP, 1 x activator and 0.2 µg/µl substrate, in presence of increasing doses of 2’3’-cGAMP (InvivoGen), 3’3’-cGAMP (InvivoGen), c-di-GMP (InvivoGen), c-di-AMP (InvivoGen), ADU-S100 (MedChemExpress), or E7766 (MedChemExpress). Incubation with 4 µM NU7441 was included as a positive control. After 1 hour, the reactions were incubated with 25 µL of ADP-Glo reagent for 40 min at room temperature, followed by incubation with 50 µL of Kinase Detection reagent for 30 min at room temperature. Luminescence was measured using the FLUOstar Omega microplate reader (BMG Labtech).

Thermal Shift Assay (TSA)

For TSA from Immunoprecipitation of purified proteins, HEK-293T cells were transfected with plasmids encoding wild-type or mutant of DNA-PKcs protein. After 48 hours, cells were lysed in TENTG-150 buffer. Anti-FLAG immunoprecipitation was performed, and proteins were eluted with FLAG peptide in TSA buffer (20 mM Tris-HCl pH 7.5, 150 mM NaCl, 5% glycerol, 1 mM DTT, 0.5 mM PMSF). For TSA from whole-cell lysate, cells were lysed in TSA buffer by five freeze-thaw cycles (liquid nitrogen / 37°). Lysates were centrifuged at 10000 rpm for 5 minutes at 4°C to remove debris. For both approaches, eluates or whole-cell lysates were incubated with water or 2',3'-cGAMP (1000 µM) on ice for 30 minutes. Samples were aliquoted (20µl) into PCR strip tubes and subjected to a thermal gradient from 46.9°C to 61.7°C for 3 minutes. Following the thermal gradient, samples were cooled on ice for 5 minutes and centrifuged at 14000 rpm for 20 minutes at 4°C. The supernatant containing soluble and non-denatured proteins was collected and mixed with Laemmli buffer before loading onto a gel for WB analysis

Flow cytometry and fluorescence microscopy of human Monocyte-Derived Macrophages upon VSV-GFP infection

1113 1x10^5 cells were seeded per well on 96 cell U-bottom plate for cytometer and on Revvity
1114 PhenoPlate 96-well for microscopy. Cells were pretreated with Nu7441(DNA-PK inhibitor) at
1115 concentration of 2 µM for one hour followed by incubation of the agonist 3'3'-cGAMP
1116 (fluorinated) at concentrations of 0.1 and 1 µg/mL for 2 hours. Then, cells were infected with
1117 VSV-GFP at MOI 0.5 and for 1 hour. Cell medium was changed and cells were either left
1118 incubated for 24h and 48h for VSV-GFP. Cells were then fixed with 4% PFA and plates were
1119 acquired either using the NovoCyte apparatus (Agilent) for flow cytometry or the Opera Phenix
1120 (Revvity) for microscopy. Flow cytometry data were then analyzed using the NovoExpress
1121 software (Agilent) while fluorescence microscopy data were analyzed with Harmony software
1122 (Revvity).

1123 Immunofluorescence analyses

1124 T98G cells grown on coverslips were transfected with 1 µg/mL 2'3'-cGAMP–iFluor 488
1125 (AAT Bioquest #20320) or DMSO (control) using JetPRIME (Sartorius). After 6 h, cells were
1126 washed with PBS, fixed with 4% formaldehyde for 20 min, then blocked/permeabilized in
1127 PBS supplemented with 0.5% Triton X-100 and 5% BSA for 1 h. Cells were incubated with anti–
1128 DNA-PK (Abcam #ab32566, 1:100) for 1 h, washed, and exposed to
1129 Alexa Fluor 594 goat anti-rabbit (Invitrogen #R37117) for 1 h. Nuclei were stained with
1130 DAPI (1 µg/mL, 10 min), then mounted with VECTASHIELD PLUS (Vector #H-1900).

1131 Confocal images were acquired on a Zeiss LSM 980 NLO. Ten to twenty images were obtained
1132 per condition with identical channel adjustments. Image analysis (CellProfiler) was used to
1133 identify 2'3'-cGAMP and DNA-PK foci (8–80 px), define cytosolic DNA-PK by inverted masks,
1134 and quantify colocalization (Relate Objects).

1135 HSV-1-KOS-64 infection in MEFs

1136 2x105 MEFs were seeded per well in a 6-well plate in a final volume of 2mL of DMEM. Cells
1137 were either infected or not with HSV-1-KOS-64 at MOI 5, then treated with either NU7441 or
1138 DMSO as control. In the first, cells were pre-treated with NU7441 then infected with HSV. In
1139 the second setup, cells were infected with HSV, then at 6hr post infection, treated with NU7441.
1140 For this condition, the two 6-well plates were collected only at 16hr post infection for qPCR
1141 analyze.

1142 Ex Vivo stimulation of primary Splenocytes

1143 Spleens were harvested from euthanized wild-type C57BL/6J mice under sterile conditions.
1144 Spleens were placed in cold RPMI-1640 medium (10% FBS, 1% penicillin-streptomycin, 2 mM

L-glutamine) and mechanically dissociated by pressing through a 70 µm cell strainer using a syringe plunger. The single-cell suspension was then collected in RPMI-1640 medium followed by lysing red blood cells with Gibco™ ACK Lysing Buffer (Thermo Fisher) according to the manufacturer's protocol. After lysis, cells were washed with washed with RPMI-1640 and filtered through 40µm trainer to remove debris. Splenocytes were used immediately to optimize cell viability. Whole splenocytes were seeded at a density of 2×10^6 cells per well in 6-well plates pretreated with 2 µM NU1744 for 1h at 37 °C or DMSO at 0.02% as a control. Subsequently, Cells were stimulated or not with STING agonists (diABZI 10 µM, 2'3'cGAMP 10µg/mL, 3'3'cGAMP 10µg/mL). After 6h at 37°C, cells were centrifuged at 300 × g for 5 minutes at 4 °C, the supernatant was stored at -80°C for a multiplex cytokines assay using the LEGENDplex™ Muli-Analyte Flow Assay Kit (Biolegend Cat. No. 740622). The remaining cell pellets were resuspended in TRIzol® Reagent (Invitrogen 15596018) for gene expression analysis as described above.

Molecular Modelling Analyses

3D coordinates were obtained from the X-ray solved, Crystal Structure of Human DNA-dependent Protein Kinase Catalytic Subunit (DNA-PKcs) with RCSB code: 5LUQ. The full amino acid sequence for ATM, ATR and mouse DNA-PK were obtained from GenBank database. The sequence alignment was done using ClustalW. The alignment was repeated using Hidden Markov Models yielding similar results as obtained by ClustalW, due to the conservation of several anchoring motifs throughout the alignment. Molecular docking studies were executed using the ZDOCK suite, which relies on a three-dimensional fast Fourier transformation algorithm. ZDOCK uses a scoring function that returns electrostatic, hydrophobic and desolvation energies, and performs a fast pairwise-shape complementarity evaluation. Moreover, it uses the contact propensities of transient complexes to perform an evaluation of a pairwise atomic statistical potential for the docking molecular system.

RDOCK was utilized to refine and evaluate the results obtained by ZDOCK. RDOCK performs a fast energy minimization step to the ZDOCK molecular complex outputs and ranks them according to their re-calculated binding free energies. Energy minimizations were used to remove any residual geometrical strain in each molecular system, using the Amber99 force field as it is implemented into the Gromacs suite, version 4.5.5. All Gromacs-related simulations were performed through our previously developed graphical interface. An implicit Generalized Born (GB) solvation was chosen at this stage, to accelerate the energy minimization process. Subsequently, molecular systems were subjected to unrestrained Molecular Dynamics Simulations (MDS) using the Gromacs suite, version 4.5.5. MDS took place in a simple point charge (SPC) water-solvated, periodic environment. Water molecules

were added using the truncated octahedron box extending 7Å from each atom. Molecular systems were neutralized with counter-ions as required. For the purposes of this study all MDS were performed using the NVT ensemble (i. e. constant Number of atoms, Volume and Temperature throughout the simulation) in a canonical environment, at 300 K and a step-size equal to 2 femto-seconds for a total 10 nanoseconds simulation time.

The quality and reliability of produced models in terms of 3D structural conformation was evaluated using the Gromacs package using a residue packing quality function, which depends on the number of buried non-polar side chain groups and on hydrogen bonding and the PROCHECK suite. Finally, the Molecular Operating Environment (MOE) suite was used to evaluate the 3D geometry of the models in terms of their Ramachandran plots, omega torsion profiles, phi/psi angles, planarity, C-beta torsion angles and rotamer strain energy profiles.

HSV-1-GFP and VSV-GFP production, infection, quantification and imaging in T98G cells:

The HSV-1 KOS-64-GFP strain (HSV-1-GFP) was a gift from S. R. Paludan (Aarhus university, Danemark). HSV-1 was amplified on Vero cells, aliquoted and frozen at -80°C. Titration was performed on Vero cells, by serial dilutions and plaque formation assessment to determine the multiplicity of infection (MOI).

VSV-GFP was a gift from Dr Sebastien Pfeffer (IBMC, France). VSV-GFP was amplified on BHK21 cells, aliquoted and frozen at -80°C. Single-round titration of the viral stock was performed on NIH-3T3 cells to determine the MOI.

$2x10^4$ T98G cells were seeded in 96 well plates in technical triplicates. The next morning, cells were pretreated or not for 1h with 2µM of NU7441. Cells were subsequently treated for 6h with either 10µM of diABZi, 1µM of E7766 or 10µg/ml of fluorinated 3’3’-cGAMP in the presence or not of 2µM NU7441. The cells were then infected with either HSV-1-GFP (for 1.5 h at MOI 2) or VSV-GFP (for 1 h at MOI 0.1) in DMEM without serum. Media was then replaced with either DMEM-10% FBS (VSV-GFP) or DMEM-1% human serum overnight and replaced with DMEM-10% FBS the next morning (HSV-1-GFP). Cells were fixed with 4% PFA for 20 min either 16 h post-infection (for VSV-GFP) or 48 h post-infection (for HSV-1-GFP). Cells were permeabilized with 0.2% Triton X-100 for 10 minutes at room temperature and nuclei were stained with DAPI.

The percentage of infected cells (i.e. GFP-positive cells) was quantified using an ImageXpress Pico (Molecular Devices) with a 4X lens. Values were averaged between technical triplicates.

Quantifications and analyses of VSV-GFP infection in human primary monocyte-derived macrophages (MDM)

Human MDM (1x10^5 cells) were pretreated with NU7441 (2 µM) for one hour, and then washed with PBS before adding the STING agonists 3'3'-cGAMP(fluorinated) (10 µg/mL) for three hours. Cells were washed again in PBS, and infections were performed with VSV-GFP (MOI of 0.5) for one hour. Finally, cells were washed from viral inputs and incubated back into Iscove's Modified Dulbecco's Medium (IMDM) (Dutscher, Bernolsheim, France) for 16 hours before fixation with Paraformaldehyde (PFA) (2%). Cells were then analyzed for GFP expression by flow cytometry on a Novocyte (Agilent Technologies).

MPXV production

The MPXV clade 2b strain (MPXV/2022/FR/CMIP) was isolated from a pustular lesion of a 36-year-old French man who consulted at the Medical Center of Institut Pasteur (CMIP), in June 2022. The clinical specimen was inoculated on Vero E6 cells, whose supernatant was harvested after 3 days and tested positive for the presence of MPXV by PCR (Batejat et al., 2022, Hubert et al., 2023). The 3rd cell passage of the virus was used.

MPXV inhibition assay

The inhibition assay was adapted from (Hubert et al., 2023). T98G cells were plated at 8 × 10^3 cells per well in a µClear 96-well plate (Greiner Bio- One). The following day, cells were incubated with 2 µM of NU7441. After one hour, supernatant was removed and cells were incubated with either 10 µM diABZI, 1 µM E7766 or 10 µg/mL of fluorinated 3'3'-cGAMP with or without 2µM NU7441. After six hours, cells were washed once with PBS and MPXV clade 2b strain was added to the cells in a BSL-3 facility, at the indicated dilutions. Viral inoculum was determined to obtain a non-saturating infection (Hubert et al., 2023). Forty-eight hours later, cells were fixed for 30 min at room temperature (RT) with 4% paraformaldehyde (PFA, Electron Microscopy Sciences), washed and immunostained for MPXV antigens with rabbit polyclonal anti-VACV antibodies (PA1-7258, Invitrogen), and an Alexa Fluor 488-coupled goat anti-rabbit antibody (Invitrogen). Nuclei were stained with Hoechst (1:10,000; Invitrogen). Images were acquired with an Opera Phenix high-content confocal microscope (PerkinElmer). For each condition, infection was quantified by calculating the total area of MPXV-positive cells ($MPXV^+$ area) and the nuclei were counted using the Harmony software (PerkinElmer). The percentage inhibition of infection was calculated from the $MPXV^+$ area using the following formula:

$$100 * \left[1 - \left[\frac{(MPXV^+\ area\ with\ drug) - (mean\ area\ of\ 'non-infected' controls)}{(mean\ area\ of\ 'no\ drug'\ infected\ controls) - (mean\ area\ of\ 'non-infected' controls)}\right]\right]$$

Statistical analysis

Statistical analysis was performed using GraphPad Prism software. To compare data from two conditions, a standard unpaired two-tailed Student's t test was performed. One-way Anova with Tukey's multiple comparisons test was used to analyze the ATP hydrolyses assay. The number of replicates in each experiment are indicated in the figure legends. All data are expressed as mean ± SEM. Results were considered significant when $p < 0.05$. Ns: non-significant. *$P < 0.05$, **$P < 0.01$, ***$P < 0.001$ and ****$P < 0.0001$

Online supplemental material

Fig. S1 supports that DNA-PKcs interacts with 2'3'-cGAMP, specifically at its catalytic site. Fig. S2 shows that DNA-PKcs regulates 2'3'-cGAMP-associated STING signaling. Fig. S3 illustrates that DNA-PKcs modulates the activity of 3'3'-cGAMP. Fig. S4 reveals that DNA-PKcs regulates the activity of STING agonists in a mouse cell line. Fig. S5 indicates that inhibition of DNA-PKcs-associated CDN signaling affects the establishment of an antiviral state.

References

AYBAR-TORRES, A. A., SALDARRIAGA, L. A., PHAM, A. T., EMTIAZJOO, A. M., SHARMA, A. K., BRYANT, A. J. & JIN, L. 2024. The common Sting1 HAQ, AQ alleles rescue CD4 T cellpenia, restore T-regs, and prevent SAVI (N153S) inflammatory disease in mice. *Elife,* 13.

BATEJAT, C., GRASSIN, Q., FEHER, M., HOINARD, D., VANHOMWEGEN, J., MANUGUERRA, J. C. & LECLERCQ, I. 2022. Heat inactivation of monkeypox virus. *J Biosaf Biosecur,* 4**,** 121-123.

BJORKMAN, A., DU, L., FELGENTREFF, K., ROSNER, C., PANKAJ KAMDAR, R., KOKARAKI, G., MATSUMOTO, Y., DAVIES, E. G., VAN DER BURG, M., NOTARANGELO, L. D., HAMMARSTROM, L. & PAN-HAMMARSTROM, Q. 2015. DNA-PKcs Is Involved in Ig Class Switch Recombination in Human B Cells. *J Immunol,* 195**,** 5608-15.

BLACKFORD, A. N. & JACKSON, S. P. 2017. ATM, ATR, and DNA-PK: The Trinity at the Heart of the DNA Damage Response. *Mol Cell,* 66**,** 801-817.

BURDETTE, D. L., MONROE, K. M., SOTELO-TROHA, K., IWIG, J. S., ECKERT, B., HYODO, M., HAYAKAWA, Y. & VANCE, R. E. 2011. STING is a direct innate immune sensor of cyclic di-GMP. *Nature,* 478**,** 515-8.

BURLEIGH, K., MALTBAEK, J. H., CAMBIER, S., GREEN, R., GALE, M., JR., JAMES, R. C. & STETSON, D. B. 2020. Human DNA-PK activates a STING-independent DNA sensing pathway. *Sci Immunol,* 5.

CORRALES, L., GLICKMAN, L. H., MCWHIRTER, S. M., KANNE, D. B., SIVICK, K. E., KATIBAH, G. E., WOO, S. R., LEMMENS, E., BANDA, T., LEONG, J. J., METCHETTE, K., DUBENSKY, T. W., JR. & GAJEWSKI, T. F. 2015. Direct Activation of STING in the Tumor Microenvironment Leads to Potent and Systemic Tumor Regression and Immunity. *Cell Rep,* 11**,** 1018-30.

DAVIES, B. W., BOGARD, R. W., YOUNG, T. S. & MEKALANOS, J. J. 2012. Coordinated regulation of accessory genetic elements produces cyclic di-nucleotides for V. cholerae virulence. *Cell,* 149**,** 358-70.

DECOUT, A., KATZ, J. D., VENKATRAMAN, S. & ABLASSER, A. 2021. The cGAS-STING pathway as a therapeutic target in inflammatory diseases. *Nat Rev Immunol,* 21**,** 548-569.

1287 FERGUSON, B. J., MANSUR, D. S., PETERS, N. E., REN, H. & SMITH, G. L. 2012. DNA-PK is a DNA sensor
1288 for IRF-3-dependent innate immunity. *Elife,* 1**,** e00047.
1289 GUHA, S., RE, J., CHEMARIN, M., GRÉGOIRE, S., MESSAOUD-NACER, Y., CHAMMA, H., AUGEREAU, A.,
1290 BARRAT, J., ACAR, N., VILA, I. K., BOUDINOT, P. & LAGUETTE, N. 2025. Regulation of lipid
1291 metabolism is a primordial function of STING. *bioRxiv***,** 2025.11.17.688879.
1292 HARDING, S. M., BENCI, J. L., IRIANTO, J., DISCHER, D. E., MINN, A. J. & GREENBERG, R. A. 2017. Mitotic
1293 progression following DNA damage enables pattern recognition within micronuclei. *Nature,*
1294 548**,** 466-470.
1295 HERTZOG, J. & REHWINKEL, J. 2020. Regulation and inhibition of the DNA sensor cGAS. *EMBO Rep,* 21**,**
1296 e51345.
1297 HINES, J. B., KACEW, A. J. & SWEIS, R. F. 2023. The Development of STING Agonists and Emerging
1298 Results as a Cancer Immunotherapy. *Curr Oncol Rep,* 25**,** 189-199.
1299 HOU, Y., WANG, Z., LIU, P., WEI, X., ZHANG, Z., FAN, S., ZHANG, L., HAN, F., SONG, Y., CHU, L. & ZHANG,
1300 C. 2023. SMPDL3A is a cGAMP-degrading enzyme induced by LXR-mediated lipid metabolism
1301 to restrict cGAS-STING DNA sensing. *Immunity,* 56**,** 2492-2507 e10.
1302 HRISTOVA, D. B., OLIVEIRA, M., WAGNER, E., MELCHER, A., HARRINGTON, K. J., BELOT, A. & FERGUSON,
1303 B. J. 2024. DNA-PKcs is required for cGAS/STING-dependent viral DNA sensing in human cells.
1304 *iScience,* 27**,** 108760.
1305 HUANG, K. C., CHANDA, D., MCGRATH, S., DIXIT, V., ZHANG, C., WU, J., TENDYKE, K., YAO, H.,
1306 HUKKANEN, R., TAYLOR, N., VERBEL, D., KIM, D. S., ENDO, A., NOLAND, T. A., CHEN, Y.,
1307 MATIJEVIC, M., WANG, J., HUTZ, J., SARWAR, N., FANG, F. G. & BAO, X. 2022. Pharmacologic
1308 Activation of STING in the Bladder Induces Potent Antitumor Immunity in Non-Muscle Invasive
1309 Murine Bladder Cancer. *Mol Cancer Ther,* 21**,** 914-924.
1310 HUBERT, M., GUIVEL-BENHASSINE, F., BRUEL, T., PORROT, F., PLANAS, D., VANHOMWEGEN, J.,
1311 WIEDEMANN, A., BURREL, S., MAROT, S., PALICH, R., MONSEL, G., DIOMBERA, H., GALLIEN, S.,
1312 LOPEZ-ZARAGOZA, J. L., VINDRIOS, W., TAIEB, F., FERNANDES-PELLERIN, S., DELHAYE, M.,
1313 LAUDE, H., AROWAS, L., UNGEHEUER, M. N., HOCQUELOUX, L., POURCHER, V., PRAZUCK, T.,
1314 MARCELIN, A. G., LELIEVRE, J. D., BATEJAT, C., LEVY, Y., MANUGUERRA, J. C. & SCHWARTZ, O.
1315 2023. Complement-dependent mpox-virus-neutralizing antibodies in infected and vaccinated
1316 individuals. *Cell Host Microbe,* 31**,** 937-948 e4.
1317 JIN, L., HILL, K. K., FILAK, H., MOGAN, J., KNOWLES, H., ZHANG, B., PERRAUD, A. L., CAMBIER, J. C. &
1318 LENZ, L. L. 2011. MPYS is required for IFN response factor 3 activation and type I IFN production
1319 in the response of cultured phagocytes to bacterial second messengers cyclic-di-AMP and
1320 cyclic-di-GMP. *J Immunol,* 187**,** 2595-601.
1321 JUTTE, B. B., KROLLMANN, C., CIESLAK, K., KOERBER, R. M., BOOR, P., GRAEF, C. M., BARTOK, E.,
1322 WAGNER, M., CARELL, T., LANDSBERG, J., AYMANS, P., WENZEL, J., BROSSART, P. &
1323 TEICHMANN, L. L. 2021. Intercellular cGAMP transmission induces innate immune activation
1324 and tissue inflammation in Trex1 deficiency. *iScience,* 24**,** 102833.
1325 LEAHY, J. J., GOLDING, B. T., GRIFFIN, R. J., HARDCASTLE, I. R., RICHARDSON, C., RIGOREAU, L. & SMITH,
1326 G. C. 2004. Identification of a highly potent and selective DNA-dependent protein kinase (DNA-
1327 PK) inhibitor (NU7441) by screening of chromenone libraries. *Bioorg Med Chem Lett,* 14**,** 6083-
1328 7.
1329 LEES-MILLER, J. P., COBBAN, A., KATSONIS, P., BACOLLA, A., TSUTAKAWA, S. E., HAMMEL, M., MEEK,
1330 K., ANDERSON, D. W., LICHTARGE, O., TAINER, J. A. & LEES-MILLER, S. P. 2021. Uncovering
1331 DNA-PKcs ancient phylogeny, unique sequence motifs and insights for human disease. *Prog*
1332 *Biophys Mol Biol,* 163**,** 87-108.
1333 LI, L., YIN, Q., KUSS, P., MALIGA, Z., MILLAN, J. L., WU, H. & MITCHISON, T. J. 2014. Hydrolysis of 2'3'-
1334 cGAMP by ENPP1 and design of nonhydrolyzable analogs. *Nat Chem Biol,* 10**,** 1043-8.
1335 MARDJUKI, R., WANG, S., CAROZZA, J. A., ABHIRAMAN, G. C., LYU, X. & LI, L. 2024. Identification of
1336 extracellular membrane protein ENPP3 as a major cGAMP hydrolase, cementing cGAMP's role
1337 as an immunotransmitter. *bioRxiv*.

1338 MCWHIRTER, S. M., BARBALAT, R., MONROE, K. M., FONTANA, M. F., HYODO, M., JONCKER, N. T., ISHII,
1339 K. J., AKIRA, S., COLONNA, M., CHEN, Z. J., FITZGERALD, K. A., HAYAKAWA, Y. & VANCE, R. E.
1340 2009. A host type I interferon response is induced by cytosolic sensing of the bacterial second
1341 messenger cyclic-di-GMP. *J Exp Med,* 206**,** 1899-911.
1342 MEEK, K., DANG, V. & LEES-MILLER, S. P. 2008. DNA-PK: the means to justify the ends? *Adv Immunol,*
1343 99**,** 33-58.
1344 MORALES, A. J., CARRERO, J. A., HUNG, P. J., TUBBS, A. T., ANDREWS, J. M., EDELSON, B. T., CALDERON,
1345 B., INNES, C. L., PAULES, R. S., PAYTON, J. E. & SLECKMAN, B. P. 2017. A type I IFN-dependent
1346 DNA damage response regulates the genetic program and inflammasome activation in
1347 macrophages. *Elife,* 6.
1348 RABINOWITZ, J., VILA, I. K., LUCHSINGER, C., BERTELLI, C., SCHUSSLER, M., TAFFONI, C., CUI, B., DAI, A.
1349 Z., RASHID, M. M., CISNEROS, W. J., CORNISH, D., REDONDO, J., JACKSON-JONES, K. A.,
1350 SIMONS, L. M., LORENZO-REDONDO, R., LAGUETTE, N., HULTQUIST, J. F. & DIAZ-GRIFFERO, F.
1351 2025. The ability of SAMHD1-deficient monocytes to trigger the Type I IFN response depends
1352 on cGAS and mitochondrial DNA. *J Biol Chem,* 301**,** 110430.
1353 SCUTTS, S. R., EMBER, S. W., REN, H., YE, C., LOVEJOY, C. A., MAZZON, M., VEYER, D. L., SUMNER, R. P.
1354 & SMITH, G. L. 2018. DNA-PK Is Targeted by Multiple Vaccinia Virus Proteins to Inhibit DNA
1355 Sensing. *Cell Rep,* 25**,** 1953-1965 e4.
1356 SIMCHONI, N., KOIDE, S., LIKHITE, M., KUCHITSU, Y., KADIRVEL, S., LAW, C. S., ELICKER, B. M., KURRA,
1357 S., WONG, M. M., YUAN, B., GROSSI, A., LAXER, R. M., VOLPI, S., DISSANAYAKE, D., TAGUCHI,
1358 T., BECK, D. B., VOGEL, T. P. & SHUM, A. K. 2025. The common HAQ STING allele prevents
1359 clinical penetrance of COPA syndrome. *J Exp Med,* 222.
1360 SUN, L., WU, J., DU, F., CHEN, X. & CHEN, Z. J. 2013. Cyclic GMP-AMP synthase is a cytosolic DNA sensor
1361 that activates the type I interferon pathway. *Science,* 339**,** 786-91.
1362 SUN, W., LI, Y., CHEN, L., CHEN, H., YOU, F., ZHOU, X., ZHOU, Y., ZHAI, Z., CHEN, D. & JIANG, Z. 2009.
1363 ERIS, an endoplasmic reticulum IFN stimulator, activates innate immune signaling through
1364 dimerization. *Proc Natl Acad Sci U S A,* 106**,** 8653-8.
1365 SUN, X., LIU, T., ZHAO, J., XIA, H., XIE, J., GUO, Y., ZHONG, L., LI, M., YANG, Q., PENG, C., ROUVET, I.,
1366 BELOT, A., SHU, H. B., FENG, P. & ZHANG, J. 2020. DNA-PK deficiency potentiates cGAS-
1367 mediated antiviral innate immunity. *Nat Commun,* 11**,** 6182.
1368 TAFFONI, C., MARINES, J., CHAMMA, H., GUHA, S., SACCAS, M., BOUZID, A., VALADAO, A. C., MAGHE,
1369 C., JARDINE, J., PARK, M. K., POLAK, K., DE MARTINO, M., VANPOUILLE-BOX, C., DEL RIO, M.,
1370 GONGORA, C., GAVARD, J., BIDERE, N., SONG, M. S., PINEAU, D., HUGNOT, J. P., KISSA, K.,
1371 FONTENILLE, L., BLANCHET, F. P., VILA, I. K. & LAGUETTE, N. 2023. DNA damage repair kinase
1372 DNA-PK and cGAS synergize to induce cancer-related inflammation in glioblastoma. *EMBO J,*
1373 42**,** e111961.
1374 TAFFONI, C., STEER, A., MARINES, J., CHAMMA, H., VILA, I. K. & LAGUETTE, N. 2021. Nucleic Acid
1375 Immunity and DNA Damage Response: New Friends and Old Foes. *Front Immunol,* 12**,** 660560.
1376 VILA, I. K., GUHA, S., KALUCKA, J., OLAGNIER, D. & LAGUETTE, N. 2022. Alternative pathways driven by
1377 STING: From innate immunity to lipid metabolism. *Cytokine Growth Factor Rev,* 68**,** 54-68.
1378 WOODWARD, J. J., IAVARONE, A. T. & PORTNOY, D. A. 2010. c-di-AMP secreted by intracellular Listeria
1379 monocytogenes activates a host type I interferon response. *Science,* 328**,** 1703-5.
1380 WU, J., SONG, L., LU, M., GAO, Q., XU, S., ZHOU, P. K. & MA, T. 2024. The multifaceted functions of
1381 DNA-PKcs: implications for the therapy of human diseases. *MedComm (2020),* 5**,** e613.
1382 YANG, H., YAO, F., MARTI, T. M., SCHMID, R. A. & PENG, R. W. 2020. Beyond DNA Repair: DNA-PKcs in
1383 Tumor Metastasis, Metabolism and Immunity. *Cancers (Basel),* 12.
1384 YI, G., BRENDEL, V. P., SHU, C., LI, P., PALANATHAN, S. & CHENG KAO, C. 2013. Single nucleotide
1385 polymorphisms of human STING can affect innate immune response to cyclic dinucleotides.
1386 *PLoS One,* 8**,** e77846.
1387 YUE, X., BAI, C., XIE, D., MA, T. & ZHOU, P. K. 2020. DNA-PKcs: A Multi-Faceted Player in DNA Damage
1388 Response. *Front Genet,* 11**,** 607428.

1389 ZHANG, X., SHI, H., WU, J., ZHANG, X., SUN, L., CHEN, C. & CHEN, Z. J. 2013. Cyclic GMP-AMP containing
1390 mixed phosphodiester linkages is an endogenous high-affinity ligand for STING. *Mol Cell,* 51**,**
1391 226-35.
1392 ZHONG, B., YANG, Y., LI, S., WANG, Y. Y., LI, Y., DIAO, F., LEI, C., HE, X., ZHANG, L., TIEN, P. & SHU, H. B.
1393 2008. The adaptor protein MITA links virus-sensing receptors to IRF3 transcription factor
1394 activation. *Immunity,* 29**,** 538-50.

1395

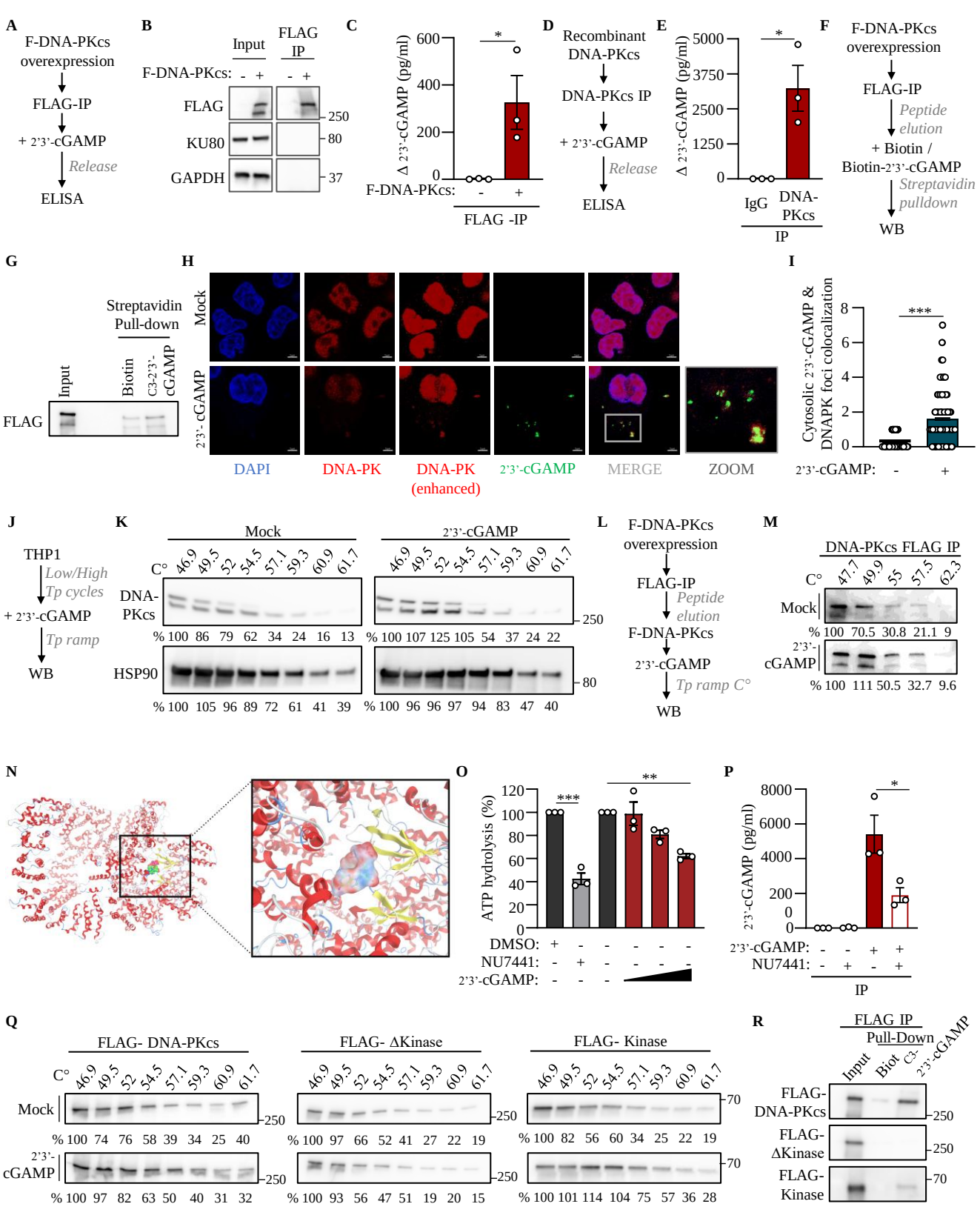
A
F-DNA-PKcs overexpression
FLAG-IP
+ 2'3'-cGAMP
Release
ELISA
B
Input
FLAG IP
F-DNA-PKcs: - + - +
FLAG
KU80
GAPDH
250
80
37
C
Δ 2'3'-cGAMP (pg/ml)
600
400
200
0
*
F-DNA-PKcs: - +
FLAG -IP
D
Recombinant DNA-PKcs
DNA-PKcs IP
+ 2'3'-cGAMP
Release
ELISA
E
Δ 2'3'-cGAMP (pg/ml)
5000
3750
2500
1250
0
*
IgG
DNA-PKcs
IP
F
F-DNA-PKcs overexpression
FLAG-IP
Peptide elution
+ Biotin / Biotin-2'3'-cGAMP
Streptavidin pulldown
WB
G
Streptavidin Pull-down
Input
Biotin
C3-2'3'-cGAMP
FLAG
H
Mock
2'3'- cGAMP
DAPI
DNA-PK
DNA-PK (enhanced)
2'3'-cGAMP
MERGE
ZOOM
I
Cytosolic 2'3'-cGAMP & DNAPK foci colocalization
8
6
4
2
0
***
2'3'-cGAMP: - +
J
THP1
Low/High Tp cycles
+ 2'3'-cGAMP
Tp ramp
WB
K
Mock
2'3'-cGAMP
C° 46.9 49.5 52 54.5 57.1 59.3 60.9 61.7
DNA-PKcs
% 100 86 79 62 34 24 16 13
% 100 107 125 105 54 37 24 22
250
HSP90
% 100 105 96 89 72 61 41 39
% 100 96 96 97 94 83 47 40
80
L
F-DNA-PKcs overexpression
FLAG-IP
Peptide elution
F-DNA-PKcs
2'3'-cGAMP
Tp ramp C°
WB
M
DNA-PKcs FLAG IP
C° 47.7 49.9 55 57.5 62.3
Mock
% 100 70.5 30.8 21.1 9
2'3'-cGAMP
% 100 111 50.5 32.7 9.6
N
O
ATP hydrolysis (%)
120
100
80
60
40
20
0
***
**
DMSO: + - - - - -
NU7441: - + - - - -
2'3'-cGAMP: - - - ▲
P
2'3'-cGAMP (pg/ml)
8000
6000
4000
200
0
*
2'3'-cGAMP: - - + +
NU7441: - + - +
IP
Q
FLAG- DNA-PKcs
FLAG- ΔKinase
FLAG- Kinase
C° 46.9 49.5 52 54.5 57.1 59.3 60.9 61.7
Mock
% 100 74 76 58 39 34 25 40
% 100 97 66 52 41 27 22 19
% 100 82 56 60 34 25 22 19
250
70
2'3'-cGAMP
% 100 97 82 63 50 40 31 32
% 100 93 56 47 51 19 20 15
% 100 101 114 104 75 57 36 28
R
FLAG IP Pull-Down
Input
Biot
C3-2'3'-cGAMP
FLAG-DNA-PKcs
FLAG-ΔKinase
FLAG-Kinase
250
250
70

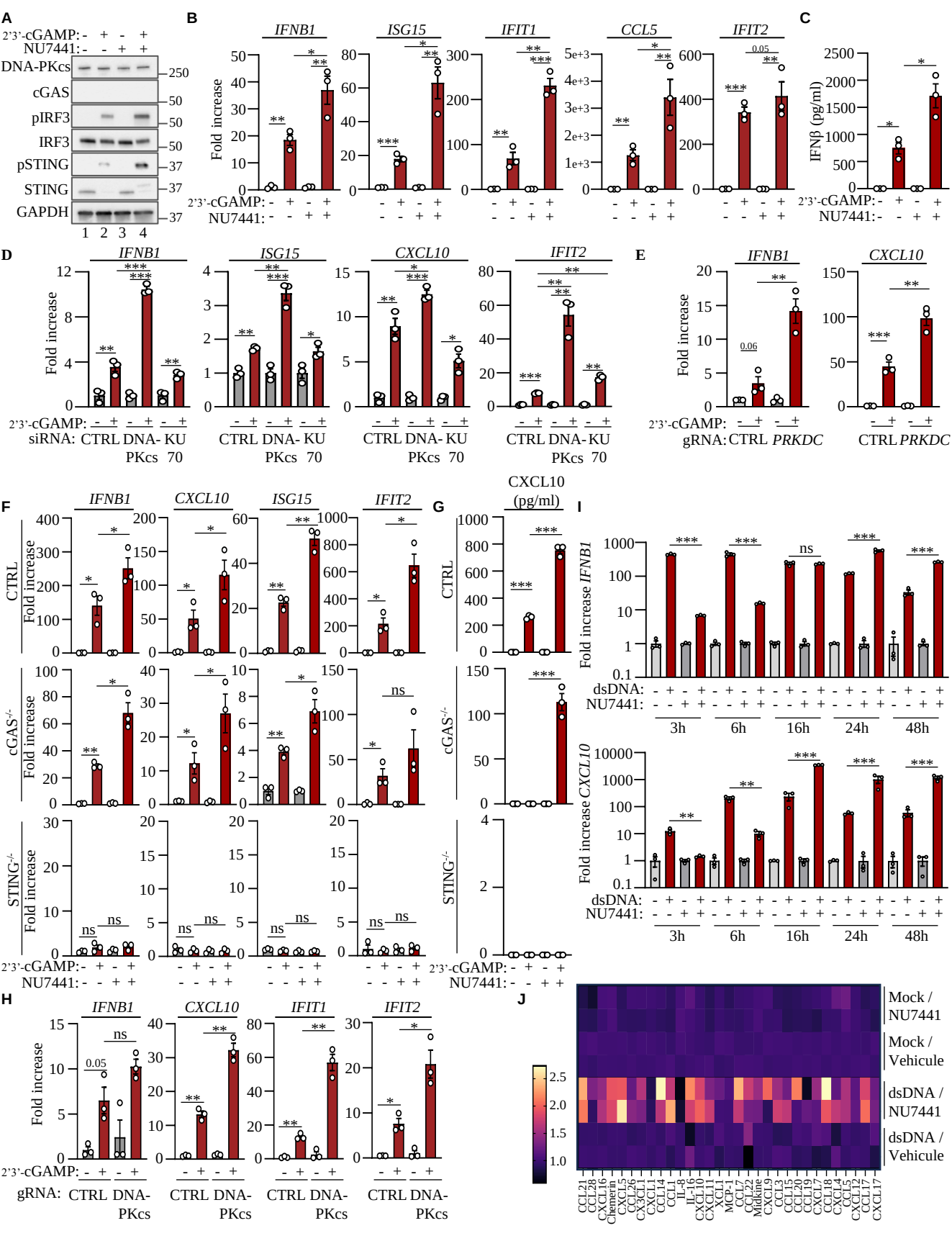
A
2'3'-cGAMP: - + - +
NU7441: - - + +
DNA-PKcs
cGAS
pIRF3
IRF3
pSTING
STING
GAPDH
250
50
50
50
37
37
37
1 2 3 4
B
IFNB1
ISG15
IFIT1
CCL5
IFIT2
Fold increase
2'3'-cGAMP: - + - +
NU7441: - - + +
C
IFNβ (pg/ml)
2'3'-cGAMP: - + - +
NU7441: - - + +
D
IFNB1
ISG15
CXCL10
IFIT2
Fold increase
2'3'-cGAMP: - + - + - +
siRNA: CTRL DNA-PKcs KU70
E
IFNB1
CXCL10
Fold increase
2'3'-cGAMP: - + - +
gRNA: CTRL PRKDC
F
IFNB1
CXCL10
ISG15
IFIT2
CTRL
cGAS-/-
STING-/-
Fold increase
2'3'-cGAMP: - + - +
NU7441: - - + +
G
CXCL10 (pg/ml)
CTRL
cGAS-/-
STING-/-
2'3'-cGAMP: - + - +
NU7441: - - + +
I
Fold increase IFNB1
Fold increase CXCL10
dsDNA: - + - + - + - + - + - + - + - + - + - +
NU7441: - - + + - - + + - - + + - - + + - - + +
3h
6h
16h
24h
48h
H
IFNB1
CXCL10
IFIT1
IFIT2
Fold increase
2'3'-cGAMP: - + - +
gRNA: CTRL DNA-PKcs
J
Mock / NU7441
Mock / Vehicule
dsDNA / NU7441
dsDNA / Vehicule
CCL21
CCL28
CXCL16
Chemerin
CXCL5
CCL26
CX3CL1
CXCL1
CCL14
CCL1
IL-8
IL-16
CXCL10
CXCL11
XCL1
MCP-1
CCL7
CCL22
Midkine
CXCL9
CCL3
CCL15
CCL20
CCL19
CXCL7
CCL18
CXCL4
CCL5
CXCL12
CCL17
CXCL17

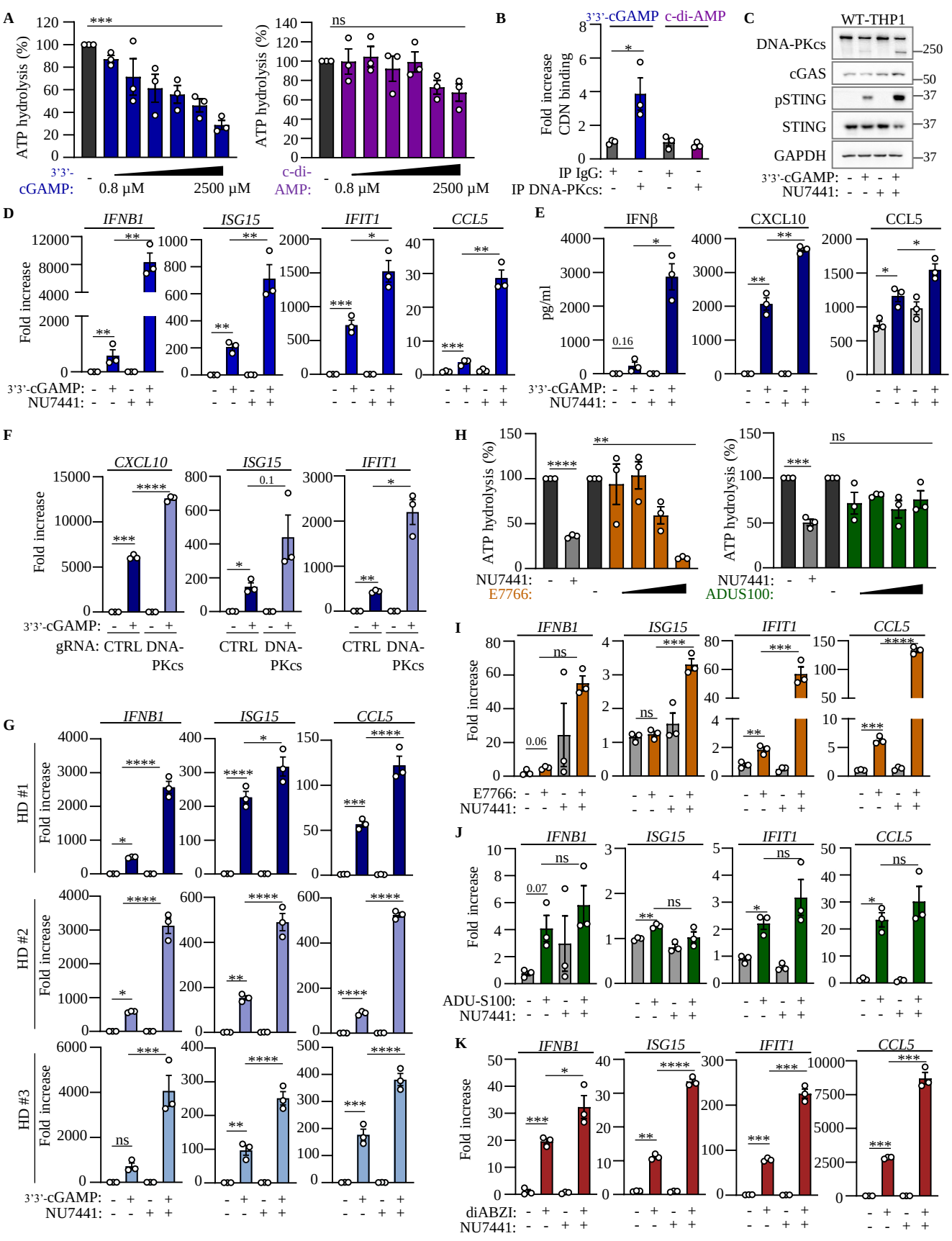
A
ATP hydrolysis (%)
***
3'3'-cGAMP:
0.8 μM
2500 μM
ns
c-di-AMP:
B
3'3'-cGAMP
c-di-AMP
Fold increase CDN binding
IP IgG:
IP DNA-PKcs:
C
WT-THP1
DNA-PKcs
cGAS
pSTING
STING
GAPDH
250
50
37
3'3'-cGAMP:
NU7441:
D
IFNB1
ISG15
IFIT1
CCL5
Fold increase
E
IFNβ
CXCL10
pg/ml
0.16
F
CXCL10
0.1
gRNA: CTRL DNA-PKcs
G
HD #1
HD #2
HD #3
H
E7766:
ADUS100:
I
0.06
J
0.07
ADU-S100:
K
diABZI:

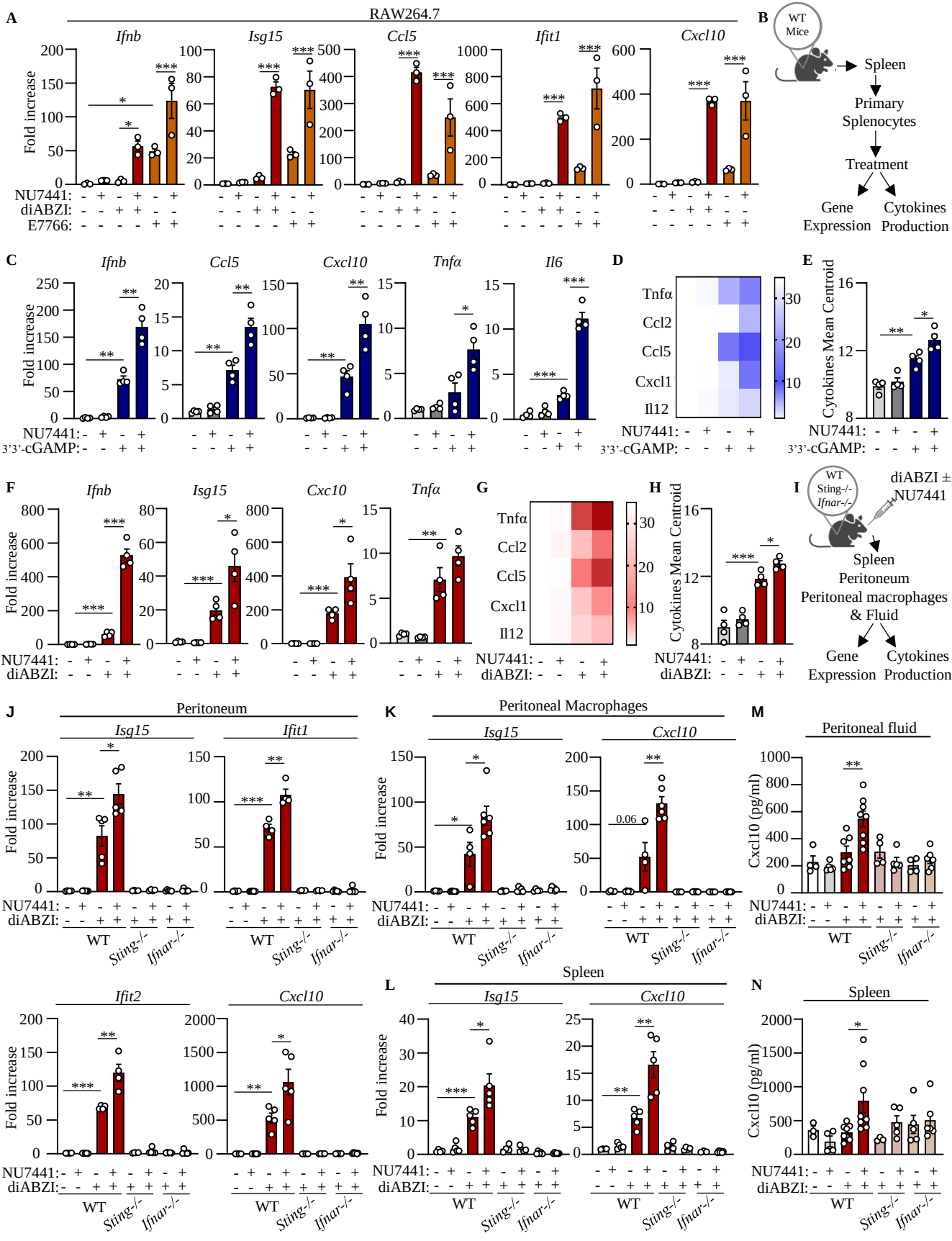
A
RAW264.7
Ifnb
Isg15
Ccl5
Ifit1
Cxcl10
Fold increase
NU7441:
diABZI:
E7766:
B
WT Mice
Spleen
Primary Splenocytes
Treatment
Gene Expression
Cytokines Production
C
Ifnb
Ccl5
Cxcl10
Tnfα
Il6
Fold increase
NU7441:
3'3'-cGAMP:
D
Tnfα
Ccl2
Ccl5
Cxcl1
Il12
NU7441:
3'3'-cGAMP:
E
Cytokines Mean Centroid
NU7441:
3'3'-cGAMP:
F
Ifnb
Isg15
Cxc10
Tnfα
Fold increase
NU7441:
diABZI:
G
Tnfα
Ccl2
Ccl5
Cxcl1
Il12
NU7441:
diABZI:
H
Cytokines Mean Centroid
NU7441:
diABZI:
I
WT Sting-/- Ifnar-/-
diABZI ± NU7441
Spleen
Peritoneum
Peritoneal macrophages & Fluid
Gene Expression
Cytokines Production
J
Peritoneum
Isg15
Ifit1
Fold increase
NU7441:
diABZI:
WT
Sting-/-
Ifnar-/-
K
Peritoneal Macrophages
Isg15
Cxcl10
Fold increase
NU7441:
diABZI:
WT
Sting-/-
Ifnar-/-
M
Peritoneal fluid
Cxcl10 (pg/ml)
NU7441:
diABZI:
WT
Sting-/-
Ifnar-/-
Ifit2
Cxcl10
Fold increase
NU7441:
diABZI:
WT
Sting-/-
Ifnar-/-
L
Spleen
Isg15
Cxcl10
Fold increase
NU7441:
diABZI:
WT
Sting-/-
Ifnar-/-
N
Spleen
Cxcl10 (pg/ml)
NU7441:
diABZI:
WT
Sting-/-
Ifnar-/-

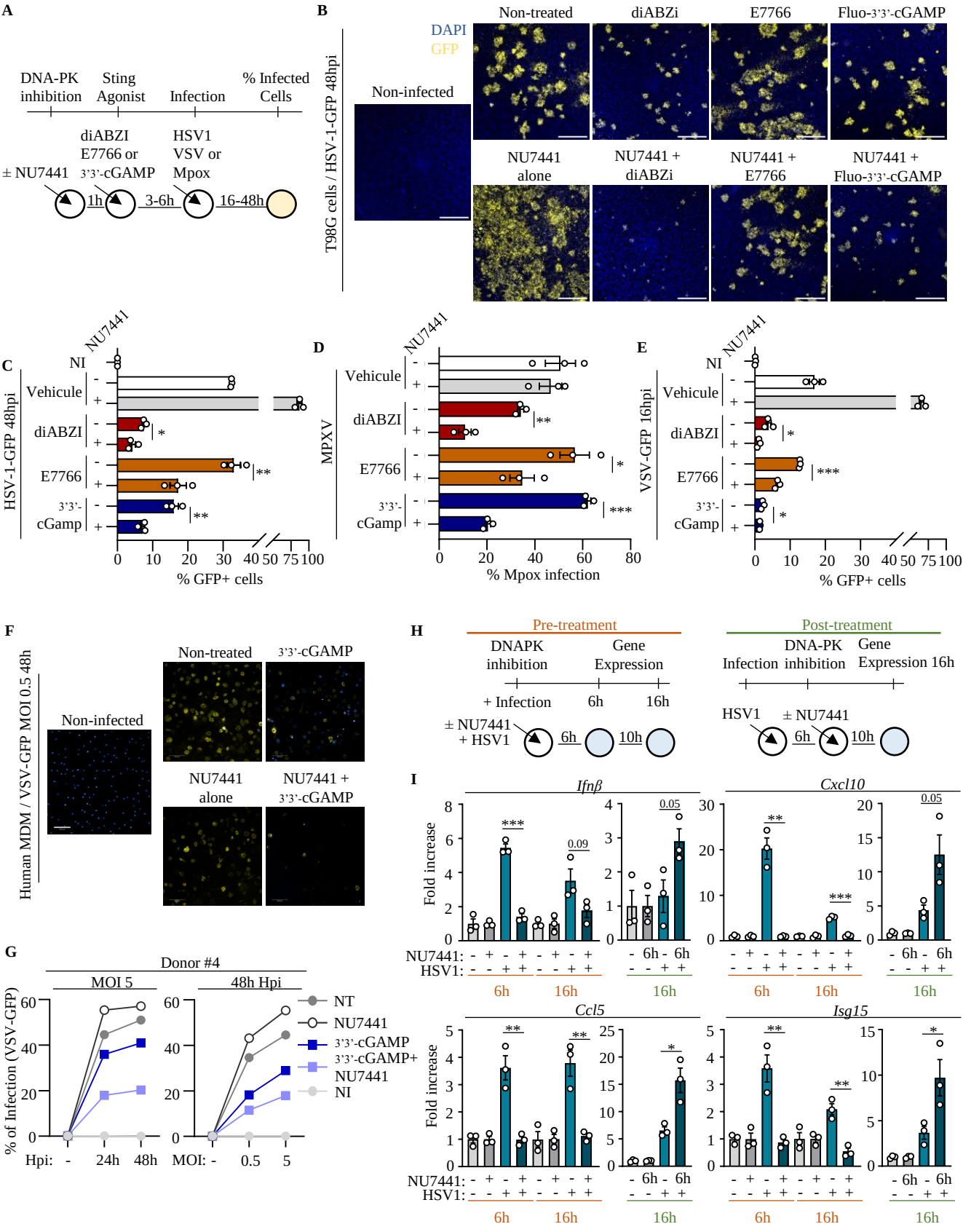
A
DNA-PK inhibition
Sting Agonist
Infection
% Infected Cells
± NU7441
diABZI E7766 or 3'3'-cGAMP
HSV1 VSV or Mpox
1h
3-6h
16-48h
B
T98G cells / HSV-1-GFP 48hpi
DAPI
GFP
Non-infected
Non-treated
diABZi
E7766
Fluo-3'3'-cGAMP
NU7441 alone
NU7441 + diABZi
NU7441 + E7766
NU7441 + Fluo-3'3'-cGAMP
C
HSV-1-GFP 48hpi
NU7441
NI
Vehicule
diABZI
E7766
3'3'-cGamp
% GFP+ cells
D
MPXV
% Mpox infection
E
VSV-GFP 16hpi
F
Human MDM / VSV-GFP MOI 0.5 48h
Non-infected
Non-treated
3'3'-cGAMP
NU7441 alone
NU7441 + 3'3'-cGAMP
G
Donor #4
MOI 5
48h Hpi
% of Infection (VSV-GFP)
Hpi:
MOI:
NT
NU7441
3'3'-cGAMP
3'3'-cGAMP+ NU7441
NI
H
Pre-treatment
DNAPK inhibition
Gene Expression
+ Infection
6h
16h
± NU7441 + HSV1
Post-treatment
DNA-PK inhibition
Infection
Gene Expression 16h
HSV1
I
Ifnβ
Cxcl10
Ccl5
Isg15
Fold increase
NU7441:
HSV1:
6h
16h

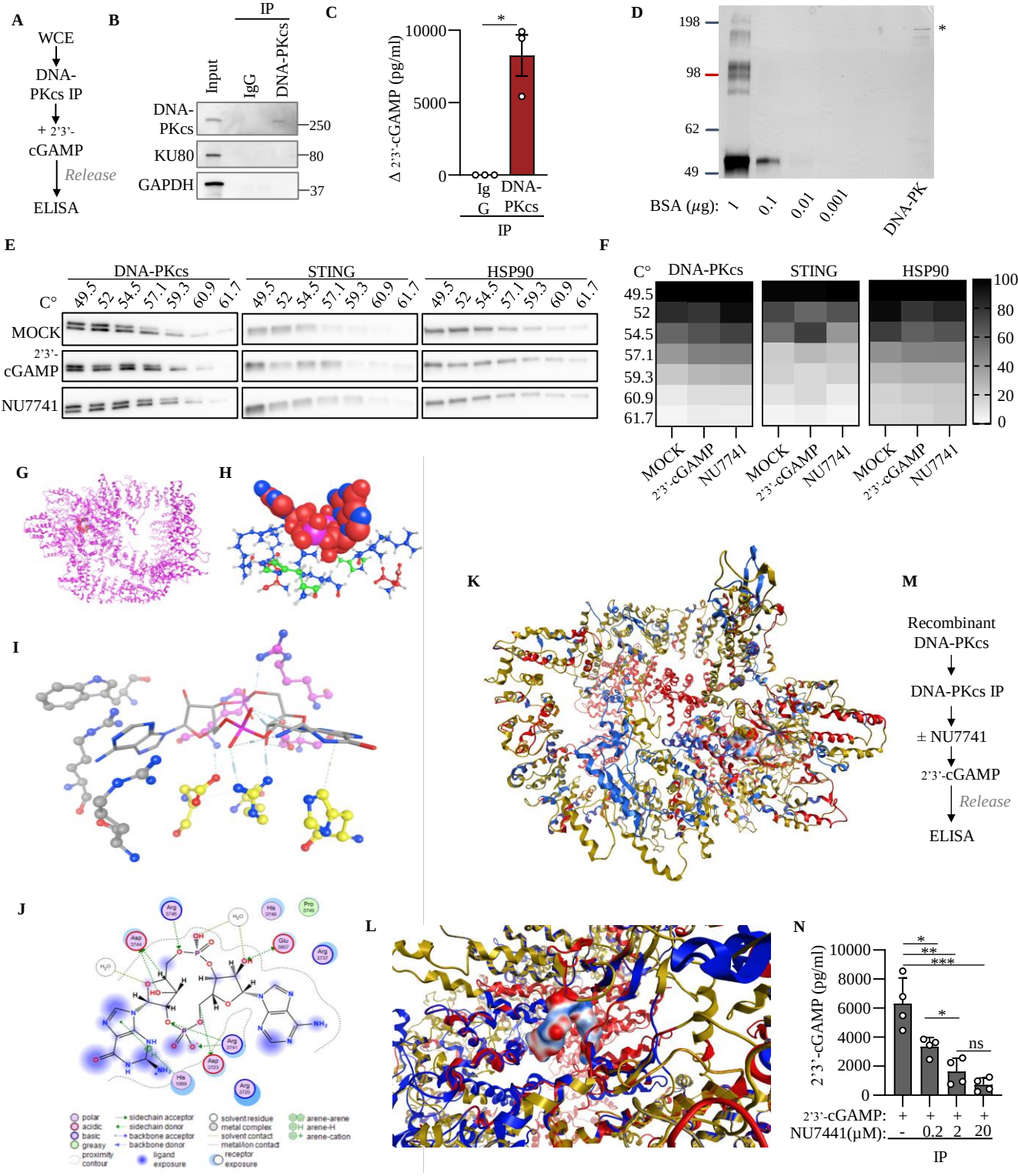
A
WCE
DNA-PKcs IP
+ 2'3'-cGAMP
Release
ELISA
B
IP
Input
IgG
DNA-PKcs
DNA-PKcs
KU80
GAPDH
250
80
37
C
Δ 2'3'-cGAMP (pg/ml)
10000
5000
0
*
Ig G
DNA-PKcs
IP
D
198
98
62
49
*
BSA (μg): 1 0.1 0.01 0.001
DNA-PK
E
DNA-PKcs
STING
HSP90
C°
49.5 52 54.5 57.1 59.3 60.9 61.7
MOCK
2'3'-cGAMP
NU7741
F
C°
DNA-PKcs
STING
HSP90
49.5
52
54.5
57.1
59.3
60.9
61.7
100
80
60
40
20
0
MOCK
2'3'-cGAMP
NU7741
G
H
I
J
K
L
M
Recombinant DNA-PKcs
DNA-PKcs IP
± NU7741
2'3'-cGAMP
Release
ELISA
N
2'3'-cGAMP (pg/ml)
10000
8000
6000
4000
2000
0
*
**
***
*
ns
2'3'-cGAMP: + + + +
NU7441(μM): - 0.2 2 20
IP

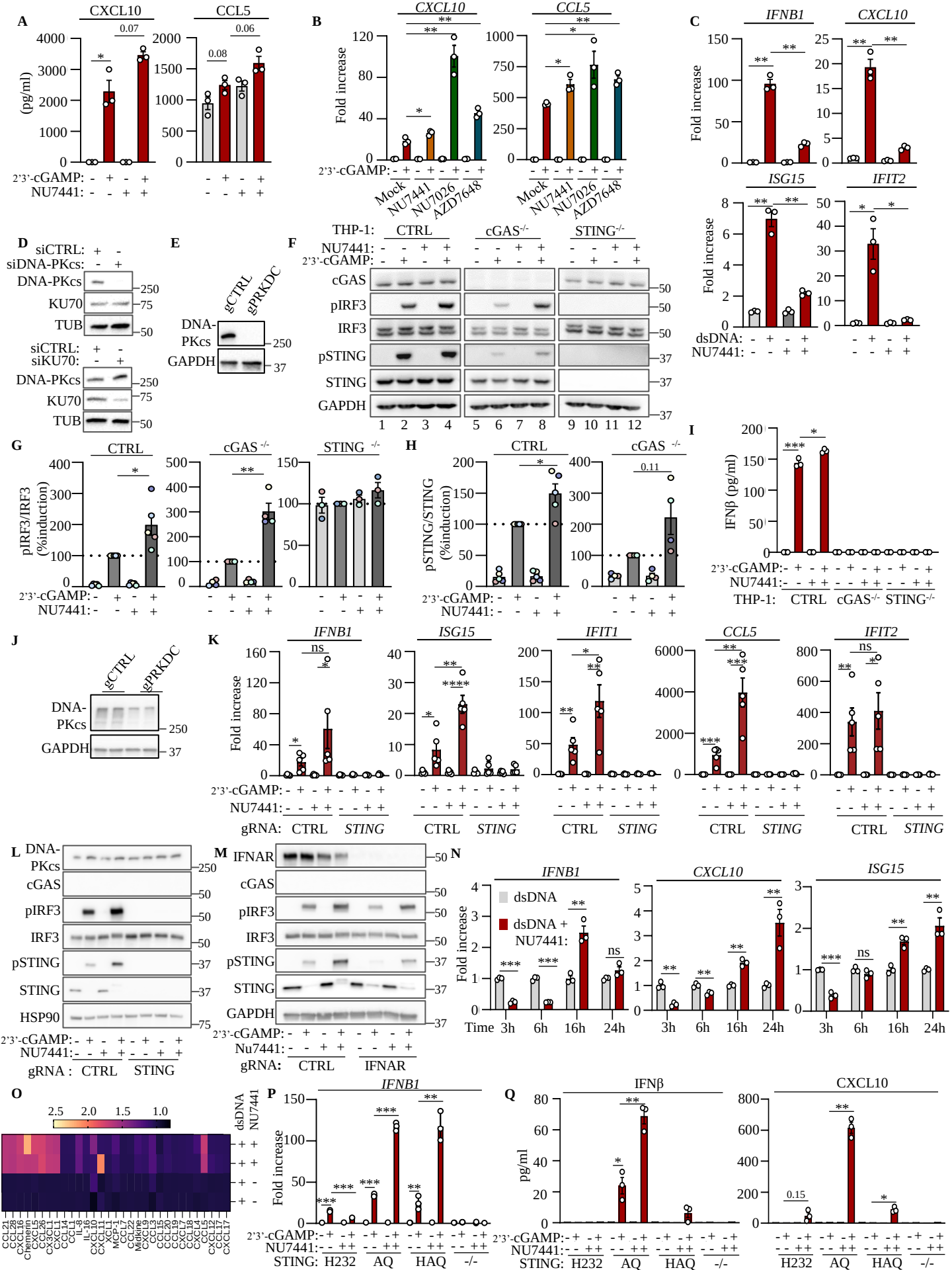

A
CXCL10
CCL5
(pg/ml)
2'3'-cGAMP:
NU7441:
B
CXCL10
CCL5
Fold increase
Mock
NU7441
NU7026
AZD7648
C
IFNB1
CXCL10
ISG15
IFIT2
Fold increase
dsDNA:
NU7441:
D
siCTRL:
siDNA-PKcs:
DNA-PKcs
KU70
TUB
siCTRL:
siKU70:
E
gCTRL
gPRKDC
DNA-PKcs
GAPDH
F
THP-1:
CTRL
cGAS-/-
STING-/-
NU7441:
2'3'-cGAMP:
cGAS
pIRF3
IRF3
pSTING
STING
GAPDH
G
CTRL
cGAS -/-
STING -/-
pIRF3/IRF3 (%induction)
H
CTRL
cGAS -/-
pSTING/STING (%induction)
I
IFNβ (pg/ml)
THP-1:
CTRL
cGAS-/-
STING-/-
J
gCTRL
gPRKDC
DNA-PKcs
GAPDH
K
IFNB1
ISG15
IFIT1
CCL5
IFIT2
Fold increase
gRNA:
CTRL
STING
L
DNA-PKcs
cGAS
pIRF3
IRF3
pSTING
STING
HSP90
gRNA :
CTRL
STING
M
IFNAR
cGAS
pIRF3
IRF3
pSTING
STING
GAPDH
gRNA:
CTRL
IFNAR
N
IFNB1
CXCL10
ISG15
dsDNA
dsDNA + NU7441:
Fold increase
Time
3h
6h
16h
24h
O
dsDNA
NU7441
CCL21
CCL28
CXCL16
Chemerin
CXCL5
CCL26
CX3CL1
CXCL1
CCL14
CCL1
IL-8
IL-16
CXCL10
CXCL11
XCL1
MCP-1
CCL7
CCL22
Midkine
CXCL9
CCL3
CCL15
CCL20
CCL19
CXCL7
CCL18
CXCL4
CCL5
CXCL12
CXCL17
CXCL17
P
IFNB1
Fold increase
STING:
H232
AQ
HAQ
-/-
Q
IFNβ
CXCL10
pg/ml
STING:
H232
AQ
HAQ
-/-

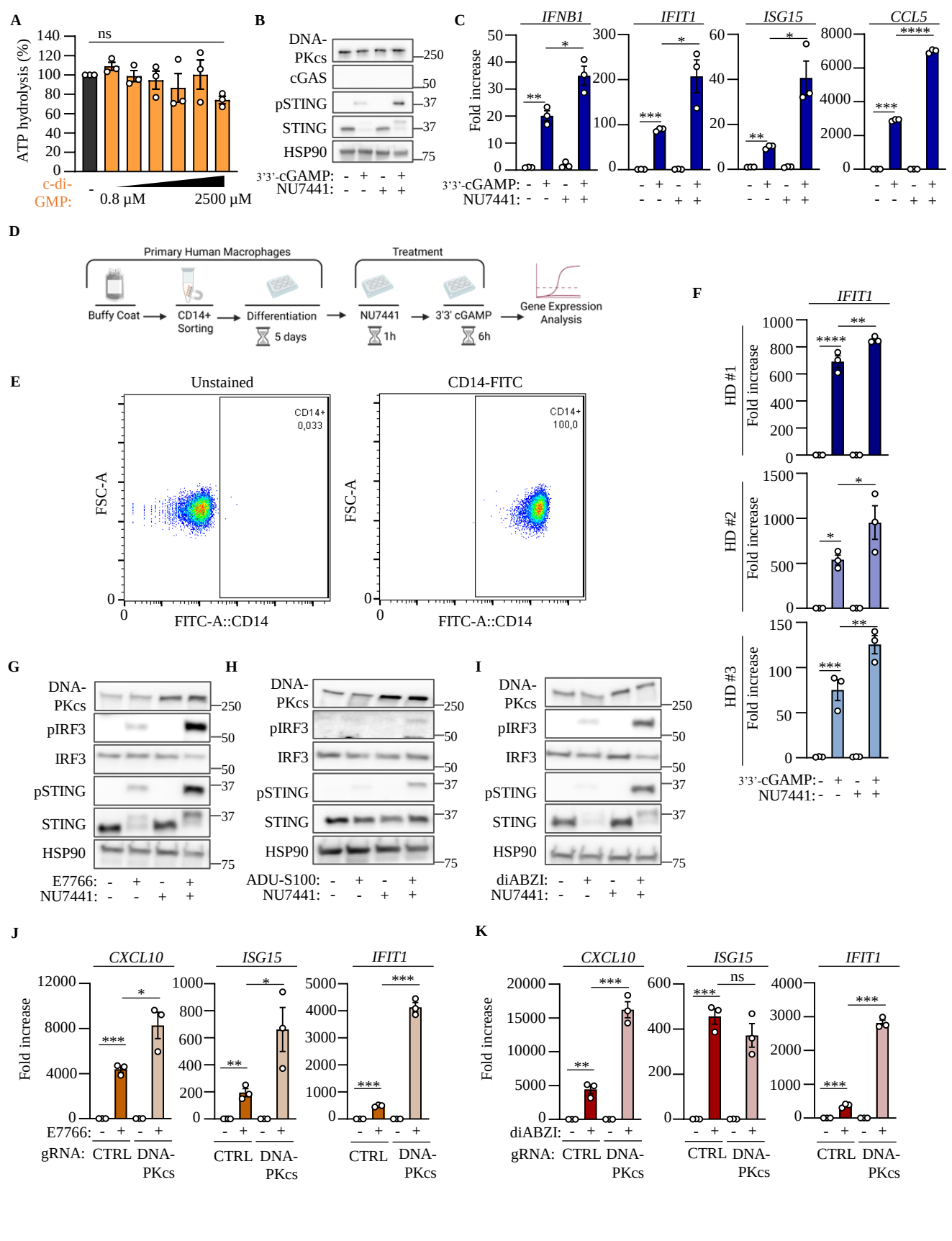
A
ATP hydrolysis (%)
ns
c-di-GMP:
0.8 µM
2500 µM
B
DNA-PKcs
cGAS
pSTING
STING
HSP90
3'3'-cGAMP:
NU7441:
C
IFNB1
IFIT1
ISG15
CCL5
Fold increase
3'3'-cGAMP:
NU7441:
D
Primary Human Macrophages
Treatment
Buffy Coat
CD14+ Sorting
Differentiation
5 days
NU7441
1h
3'3' cGAMP
6h
Gene Expression Analysis
E
Unstained
CD14-FITC
CD14+ 0,033
CD14+ 100,0
FSC-A
FITC-A::CD14
F
IFIT1
HD #1
HD #2
HD #3
Fold increase
3'3'-cGAMP:
NU7441:
G
DNA-PKcs
pIRF3
IRF3
pSTING
STING
HSP90
E7766:
NU7441:
H
ADU-S100:
NU7441:
I
diABZI:
NU7441:
J
CXCL10
ISG15
IFIT1
Fold increase
E7766:
gRNA:
CTRL
DNA-PKcs
K
diABZI:
gRNA:

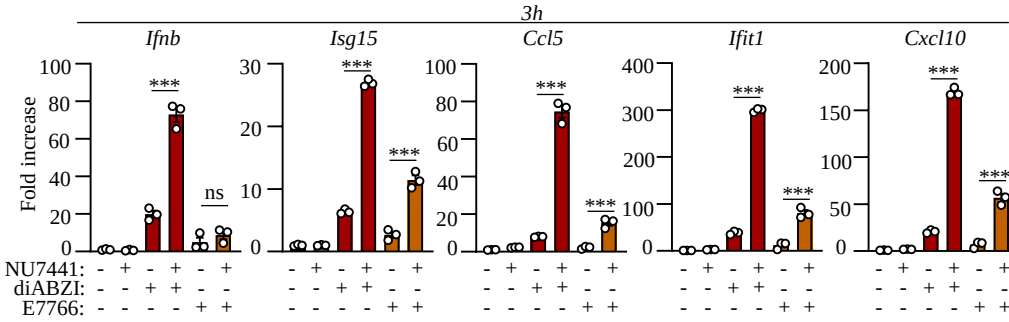
3h
Ifnb
Isg15
Ccl5
Ifit1
Cxcl10
Fold increase
***
ns
NU7441:
diABZI:
E7766:

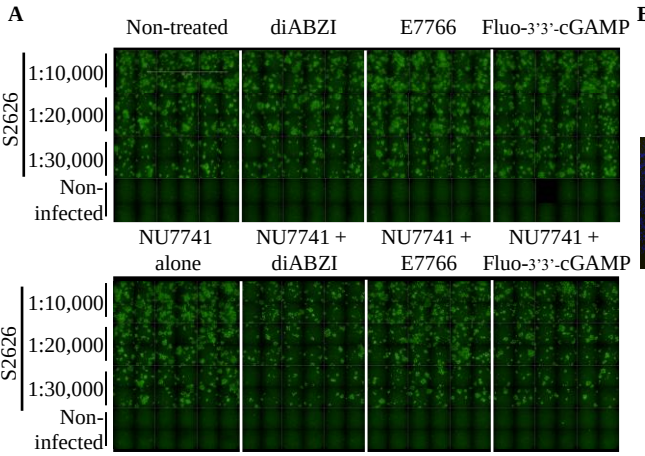

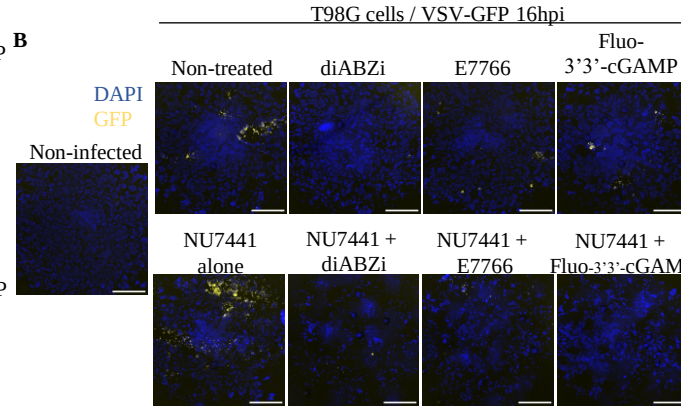

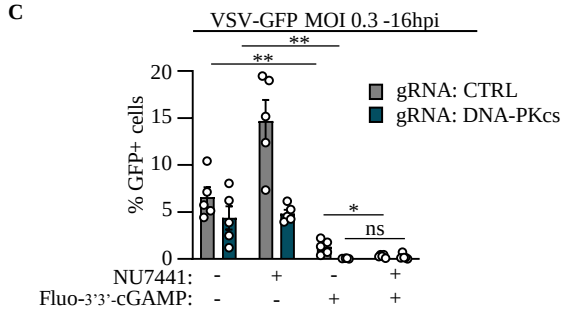

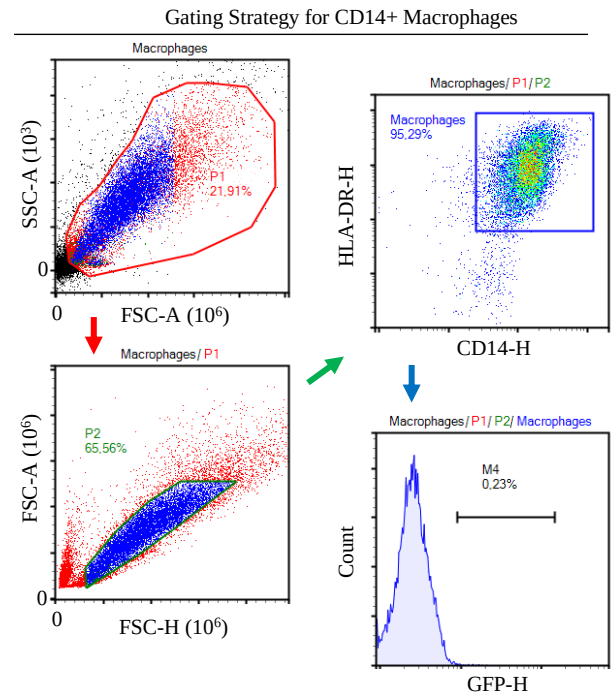

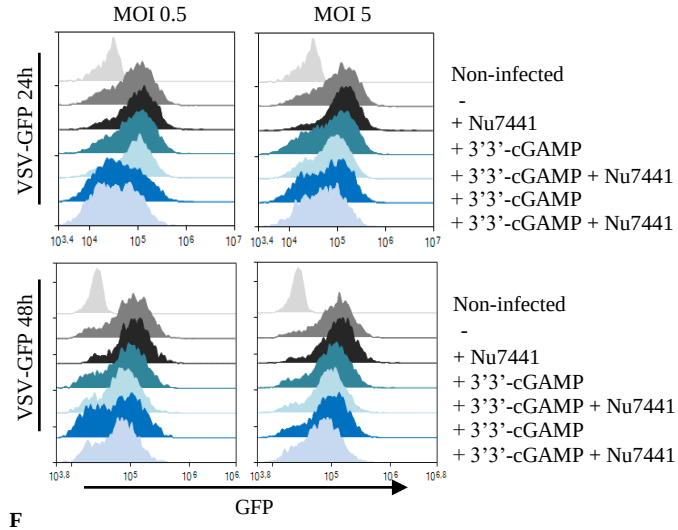

F

VSV MOI 5 –16hpost infection	Impact of NU7441 on % VSV infected cells			
	HD#1	HD#2	HD#3	p.value
Non-Treated	100	100	100	0.002
NU7441	132.6	134	150.2	
diABZi	100	100	100	0.002
diABZi + NU7441	40.5	62.9	57.9	
E7766	100	100	100	0.008
E7766 + NU7441	57.7	73.2	43.6	
3'3'-cGAMP	100	100	100	0.038
3'3'-cGAMP + NU7441	52.5	59.7	88.2	